Electrophysiological recording from *Xenopus* oocytes

Potassium currents were recorded under a two-electrode voltage clamp using an OC-725C amplifier (Warner Instruments, Hamden, CT, USA) and Clampex 10.3 software (Molecular Devices, Sunnyvale, CA, USA). The signals were digitized at 10 kHz using a Digidata 1322A (Molecular Devices). The microelectrodes were filled with an electrode solution containing 3 M potassium acetate and 10 mM KCl. The oocytes were perfused with a bath solution containing (mM): 96 NaCl, 2 KCl, 1.8 $CaCl_2$, 1 $MgCl_2$ and 5 Hepes (pH adjusted to 7.2 with NaOH). All experiments were performed at 25°C. The data were analysed using Clampfit 10.3 software (Molecular Devices) and Igor Pro 6 software (Wavemetrics, Lake Oswego, OR, USA) with the added import functionality provided by the ReadPclamp XOP of the NeuroMatic software package (http://www.neuromatic.thinkrandom.com/). To calculate conductance–voltage relationships, outward currents were activated by applying 1000 ms voltage steps from a holding potential of −80 mV to potentials up to +70 mV in 10 mV increments. The equilibrium potential of K^+ ($E_K = -104.0$ mV) was calculated from the intracellular concentration of K^+ (109.5 mM) in the *Xenopus* oocyte (Costa *et al.* 1989). To determine steady-state inactivation, cells were held at −80 mV before applying a 1000 ms prepulse to potentials between −80 and +60 mV in 10 mV increments, followed by a 250 ms test pulse to +20 mV. Steady-state inactivation (I/I_{max}) curves were fitted with the Boltzmann function, $I/I_{max} = 1/[1 + \exp(V - V_{\frac{1}{2}})/k]$, where k is a slope factor. To measure the rates of deactivation, outward currents were evoked by stepping from a holding potential of −80 mV to +50 mV for 5 ms and then stepping to potentials between −60 and +10 mV in 10 mV increments for 50 ms. The time constant of recovery (τ_{recove}) from inactivation was determined by depolarizing the cells to +50 mV for 1000 ms from a holding potential of −80 mV. A step to −80 mV of variable duration was followed with test pulses to +50 mV for 200 ms in 500 ms increments. The data points were fitted with a single exponential function. The time constants of inactivation (τ_{inacti}) and deactivation were obtained by fitting current traces with a single exponential function on the inactivating and deactivating phases of the traces, respectively.

Whole-cell patch-clamp recordings from cultured PCs

In most recordings, cerebellar cultures were constantly perfused (2 ml min^{-1}) with oxygenated artificial cerebrospinal fluid (ACSF) containing (mM): 120 NaCl, 2.5 KCl, 2 $CaCl_2$, 1 $MgCl_2$, 26 $NaHCO_3$, 1.25 NaH_2PO_4, 17 D-glucose and 0.1 picrotoxin (Tocris Bioscience, Bristol, UK; a $GABA_A$ receptor antagonist), bubbled with 5% CO_2–95% O_2 at 26°C. The other recordings were performed in Hepes-buffered ACSF containing (mM): 140 NaCl, 2.5 KCl, 2 $CaCl_2$, 1 $MgCl_2$, 10 D-glucose and 10 Hepes (pH adjusted to 7.4 with NaOH), bubbled with 100% O_2. Outward currents were recorded in Hepes-buffered ACSF containing (mM): 0.2 $CdCl_2$, 0.1 picrotoxin, 0.05 6,7-dinitroquinoxaline-2,3-dione (DNQX; Tocris Bioscience; a AMPA/kainate receptor antagonist,) and 0.001 TTX (Wako Pure Chemical Industries). Hepes buffer was used to avoid the precipitation of $CdCO_3$.

Cells were visualized on the stage of an upright microscope (BX50WI; Olympus, Tokyo, Japan) using a ×40 water-immersion objective lens with Nomarski optics and a near-infrared CCD camera (C-3077-79; Hamamatsu Photonics, Hamamatsu, Japan). Green fluorescent protein-positive cells were visualized and selected using epifluorescence optics (Olympus). Patch pipettes were made from borosilicate glass capillaries to reduce pipette capacitance (GC150F-100; Harvard Apparatus, Holliston, MA, USA) and had a resistance of 1.5–2.5 MΩ when filled with a potassium gluconate-based internal solution containing (mM): 145 potassium gluconate, 5 KCl, 0.1 EGTA, 5 Mg-ATP, 5 disodium phosphocreatine, 0.3 Na_2-GTP, 10 Hepes–KOH and 10 biocytin (Sigma-Aldrich), pH 7.3. The liquid junction potential (−10 mV) was corrected offline. Whole-cell patch-clamp recordings were conducted in GFP-positive PCs at DIV 8–10. Purkinje cells were identifiable by their large somatic size (Tabata *et al.* 2000), and their identity was confirmed by intracellular staining with biocytin. Patch-clamp recordings were acquired using a Multiclamp 700B amplifier with Clampex 10.3 software (Molecular Devices). Signals were filtered at 6–10 kHz and digitized at 10–50 kHz using a Digidata 1440A (Molecular Devices). In voltage-clamp conditions, series resistance was compensated electronically by 80–90%, and in current-clamp conditions, it was performed using the bridge balance and capacitance neutralization. Outward currents were activated with 500 ms voltage steps from −70 mV to voltages ranging from −60 to +40 mV in 10 mV increments. Leak currents were subtracted online by the *P*/4 protocol (Armstrong & Bezanilla, 1974). The recorded currents were normalized to cell capacitance, which was calculated from the transient current evoked by applying a small voltage step (−5 mV, 20 ms duration) from a holding potential of −70 mV in voltage-clamp conditions. Spontaneous excitatory post-synaptic currents (sEPSCs) were recorded at a holding potential of −80 mV for 250 s in the presence of picrotoxin and detected offline using the template search function in the Clampfit 10.3 software. Action potentials were evoked by depolarizing current pulses in current-clamp conditions (10 ms duration, from 0 to 200 pA in 10 pA increments; or 200 ms duration, from 0 to 200 pA in 20 pA increments). The resting membrane potentials were

adjusted to −60 mV by current injection. Spontaneous firing was recorded at resting membrane potential for 300 s. The half-amplitude width of the action potential was measured at the mid-point between the threshold and peak. Action potential amplitude was measured between the threshold and peak.

Fluorescence imaging of calcium

To monitor the free $[Ca^{2+}]_i$ of PCs, cerebellar cultures at DIV 8–10 were incubated with Hepes-buffered ACSF containing fura-2 AM (0.01 mM; Invitrogen) for 1 h at 37°C. The cells were visualized and perfused with Hepes-buffered ACSF at the same settings as those used for the patch-clamp recordings. For fura-2 excitation, the cultures were illuminated alternately at 340 and 380 nm wavelengths using a 100 W xenon lamp source, a fura-2 filter set (ET FURA2; Chroma Technology, Brattleboro, VT, USA), and a filter wheel (Ludl Electronic Products, Hawthorne, NY, USA). The fluorescence was filtered through a bandpass filter (470–550 nm) and captured using an EMCCD camera (iXon3 DU897; Andor Technology, Belfast, UK). The experiments were controlled by Andor iQ software (Andor Technology). The regions of interest were defined as the shape of the GFP-expressing Purkinje cell bodies. The $[Ca^{2+}]_i$ was calculated according to the previously described method with a dissociation constant of 224 nM (Grynkiewicz *et al.* 1985). The maximal and minimal fluorescence ratios (R_{max} and R_{min}) were measured after addition of the calibration solutions. The R_{max} was measured in Hepes-buffered ACSF containing 5 μM ionomycin (Sigma-Aldrich), and R_{min} in Hepes-buffered, Ca^{2+}-free ACSF containing 10 mM EGTA and 5 μM ionomycin. In some experiments, the cultures were perfused for 5 min with high-K^+ ACSF, in which 12.5 mM NaCl was replaced by equimolar KCl (total $[K^+]$, 15 mM) to elevate $[Ca^{2+}]_i$. Basal $[Ca^{2+}]_i$ was obtained as an average for a 7 min period from the beginning of the recordings, and elevated $[Ca^{2+}]_i$ for a 5 min period during high-K^+ ACSF perfusion.

Results

R424H mutant subunits exhibit a dominant-negative effect against WT mKv3.3 subunits without affecting WT subunit expression in heterologous expression systems

We examined whether the biophysical properties of hKv3.3 with the R423H mutation were conserved in mKv3.3 with the R424H mutation using the *Xenopus* oocyte expression system and two-electrode voltage-clamp recording (Figueroa *et al.* 2010; Minassian *et al.* 2012). In WT mKv3.3-expressing oocytes, depolarizing voltage steps from a holding potential of −80 mV evoked outward currents that became more apparent when the membrane was depolarized to potentials more positive than −10 mV (Supplemental Fig. S2*Aa* and S2*C*; a $V_{1/2}$ of activation of 25.5 ± 3.1 mV, $n = 19$), and the currents showed inactivation (Supplemental Fig. S2*Aa*, $n = 11$) and fast deactivation (deactivation $\tau = 0.948 \pm 0.15$ ms at −40 mV, $n = 11$; trace not shown). These results well reflected the reported properties of Kv3.3 channels, i.e. fast activation, positively shifted voltage dependence, N-type inactivation and a fast deactivation rate (Rae & Shepard, 2000; Rudy & McBain, 2001; Desai *et al.* 2008). In R424H mutant-expressing oocytes, negligible currents were observed at potentials more positive than +20 mV (Supplemental Fig. S2*Ac* and S2*B*), and the peak amplitudes were not significantly larger than those recorded in water-injected oocytes (Supplemental Fig. S2*B*; not significant by Student's unpaired *t* test), indicating that most of the currents were derived from endogenous channels present in *Xenopus* oocytes. When cRNA of WT and R424H mutant mKv3.3 was injected at a 1:1 ratio (WT+R424H), the $V_{1/2}$ of activation was significantly left-shifted, by 9.05 mV, compared with oocytes expressing WT subunits alone (Supplemental Fig. S2*C*; WT+R424H, 15.6 ± 9.2 mV, $n = 21$; WT, 24.6 ± 6.1 mV, $n = 19$; $P < 0.001$ by Student's unpaired *t* test). The value of k was decreased by 4.29 mV (WT + R424H, $k = 9.82 \pm 2.4$ mV, $n = 21$; WT, $k = 14.1 \pm 3.1$ mV, $n = 19$; $P < 0.001$ by Student's unpaired *t* test), and the time constant of activation (τ_{acti}) at +40 mV was 2.03-fold slower (Supplemental Fig. S2*Da* and S2*Db*; $P < 0.001$ by Student's unpaired *t* test). These results are consistent with previous reports of hKv3.3 with R423H mutation (Figueroa *et al.* 2010; Minassian *et al.* 2012) and indicate that the functional effects of this mutation are well conserved between humans and mice.

Coexpression of R424H mutant and WT subunits accelerates the inactivation kinetics and slows the recovery from inactivation compared with WT subunits alone

In order to reveal further the unknown biophysical properties of hKv3.3 with the R423H mutation, we investigated the inactivation kinetics, steady-state inactivation and recovery from inactivation of WT+R424H mutant channels. The τ_{inacti} of WT+R424H mutant channels was more than 2-fold faster than that of channels composed of WT subunits alone in the range of +10 to +70 mV depolarizing steps (Fig. 1*A*), and the $V_{1/2}$ of inactivation was significantly left-shifted, by 9.67 mV, compared with that of WT subunits (Fig. 1*B*; WT+R424H, $V_{1/2} = -4.39 \pm 7.09$ mV, $n = 12$; WT, $V_{1/2} = 5.28 \pm 5.33$ mV, $n = 11$; $P < 0.01$ by

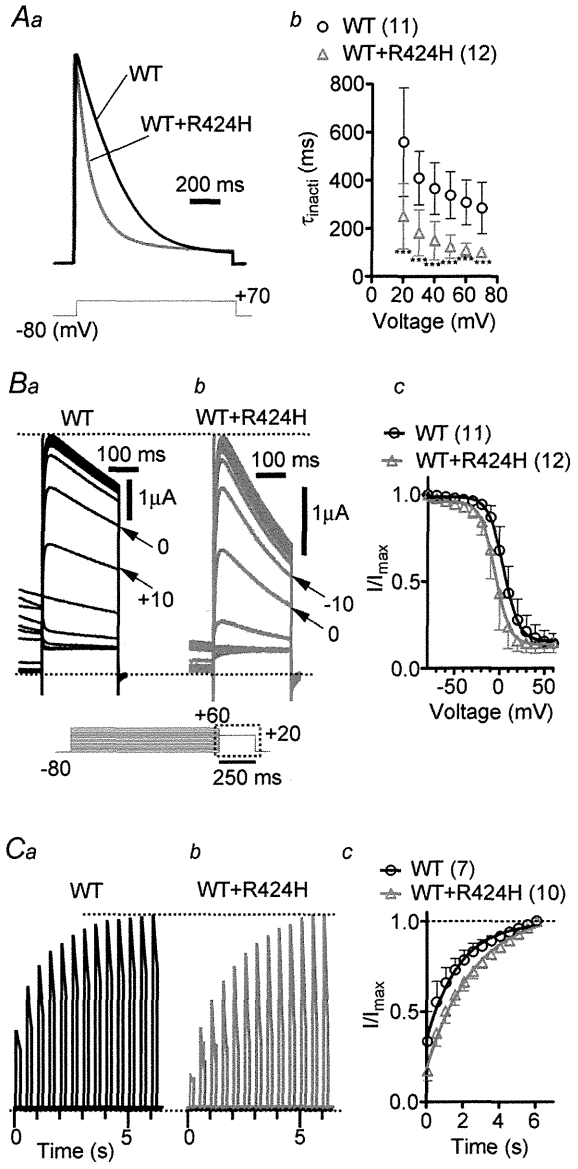

Figure 1. Coexpression of R424H mutant and wild-type (WT) subunits in *Xenopus* oocytes accelerates the inactivation kinetics and slows the recovery from inactivation compared with WT subunits alone
Aa, representative traces evoked by stepping from a −80 mV holding potential to +70 mV. The current traces are scaled to the same peak amplitude. *Ab*, the plots of the inactivation time constant (τ_{inacti}) were determined by fitting the falling phases of currents obtained in Supplemental Fig. S2*A* with a single exponential function. *Ba* and *b*, comparison of steady-state inactivation, which was obtained by changing the membrane potential from a prepulse potential ranging from −80 to +60 mV in 10 mV increments to a test voltage step of +20 mV to record tail currents. *Ba* and *b* shows traces of tail currents, and their corresponding voltage pulses are given under the traces surrounded by the dotted rectangle. *Bc*, the tail current amplitudes were normalized to the maximal current, and the resulting plots were fitted with the Boltzmann function, $I/I_{max} = 1/[1 + \exp(V - V_{1/2})/k]$, where k is a slope factor. *C*, recovery from inactivation in WT channels and WT+R424H mutant channels. *Ca* and *b*, the recovery time constant (τ_{recove}) was determined by depolarizing the cells to +50 mV for 1000 ms from a holding potential of −80 mV. A step to −80 mV of variable duration was followed with test pulses to +50 mV for 200 ms in 500 ms increments. *Cc*, time course of the recovery from inactivation. The curves were fitted with a single exponential function to obtain τ_{recove}. Here and in the following figures, error bars indicate standard deviation, the numbers in parentheses indicate the number of experiments, and statistical significance was tested using Mann-Whitney's *U* test unless otherwise stated (significance, $P < 0.05$). ***$P < 0.001$.

Student's unpaired *t* test). The τ_{recove} from inactivation of WT+R424H was significantly slower than that of WT (Fig. 1*C*; WT+R424H, $\tau_{recove} = 2.62 \pm 0.60$, $n = 10$; WT, $\tau_{recove} = 1.78 \pm 0.08$, $n = 7$; $P < 0.01$ by Student's unpaired *t* test). These results indicate that coexpression of WT and R424H mutant subunits accelerated the inactivation kinetics and slowed recovery from inactivation.

Expression of R424H mutant subunits in cerebellar cultures induces PC death and impairs dendritic development

Spinocerebellar ataxia type 13 patients show cerebellar symptoms and cerebellar atrophy, suggesting shrinkage of the cerebellar cortex and degeneration of cerebellar neurons (Waters *et al.* 2006; Figueroa *et al.* 2010, 2011). In order to explore the effects of the R424H mutant on cell survival, dendritic development and electrophysiological properties in cerebellar neurons, mouse cerebellar cultures were infected at DIV 0 with lentiviruses expressing WT or R424H mutant subunits together with GFP. Given that SCA13 is an autosomal dominant disorder and Kv3 channels are formed by the assembly of four pore-forming subunits, hKv3.3 channels in SCA13 patients are considered to be heteromultimer channels consisting of WT and mutant subunits (MacKinnon, 1991; Figueroa *et al.* 2010; Minassian *et al.* 2012). When R424H mutant subunits were lentivirally expressed in cultured PCs, the subunits were expected to incorporate into endogenous mKv3.3 channels, mimicking the pathological condition.

Green fluorescent protein fluorescence was observed after DIV 3, and >90% of PCs were GFP positive (Fig. 2*A*–*C*). In the immunohistochemical experiments, PCs were immunostained with anti-calbindin antibody and granule cells with anti-NeuN antibody. Mullen *et al.* (1992) reported that PCs are not stained with anti-NeuN antibody *in vivo*. In agreement with their report, PCs and GABAergic interneurons were NeuN negative in our culture conditions (Supplemental Fig. S3*A* and S3*B*). The mKv3.3 protein in WT-expressing PCs at DIV 10 was significantly overexpressed (by 8.3-fold) compared with that in PCs expressing GFP alone (Supplemental Fig. S3*E*). In contrast to the clear expression of mKv3.3 protein

in PCs (Goldman-Wohl *et al.* 1994), mKv3.3 expression was not detected in cultured granule cells (Supplemental Fig. S3*C*), differing from a previous report using an *in vivo* preparation (Chang *et al.* 2007). Consistent with a previous report (Tabata *et al.* 2000), the relative densities of GFP- and WT-expressing PCs decreased in a day-dependent manner (Fig. 2*A*, *B* and *D*). Until DIV 7, the relative densities of PCs did not differ significantly between R424H mutant-expressing and control cultures (Fig. 2*Aa*, *Ba*, *Ca* and *D*; $P = 0.346$ between GFP and R424H; $P = 0.222$ between WT and R424H). At DIV 11, however, the density of PCs in R424H mutant-expressing cultures was significantly decreased (Fig. 2*Ab*, *Bb*, *Cb* and *D*; $P < 0.01$ between GFP and R424H; $P < 0.01$ between WT and R424H). At DIV 14, ~40% of PCs still survived in GFP- or WT-expressing cultures (Fig. 2*Ac*, *Bc*, *Cc* and *D*), whereas there were few surviving PCs in R424H mutant-expressing cultures. Relative cell densities and the percentage of GFP-positive cells of granule cells at DIV 14 were also quantified, but there were no significant differences between R424H mutant-expressing and control cultures (Fig. 2*Ac′*, *Bc′*, *Cc′* and *E*; cell densities, $P = 0.0952$ between GFP and R424H; $P = 0.117$ between WT and R424H; and percentage of GFP-positive cells, GFP, 65.9 ± 8.3%, $n = 5$; WT, 64.0 ± 7.4%, $n = 5$; R424H, 59.8 ± 8.1%, $n = 5$; $P = 0.421$ between GFP and R424H; $P = 0.310$ between WT and R424H), indicating that expression of R424H mutant subunits did

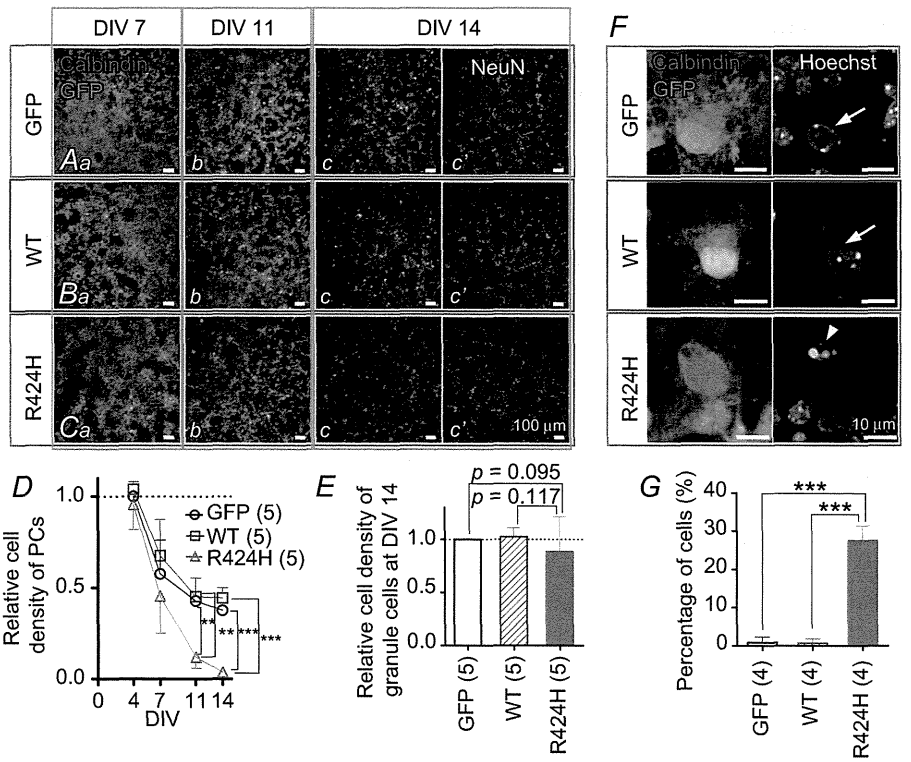

Figure 2. Lentivirus-mediated expression of R424H mutant subunits in cerebellar cultures decreases the density of Purkinje cells (PCs) but not of granule cells

A–C, immunofluorescence images of cerebellar cultures infected with lentiviral vectors expressing green fluorescent protein (GFP) alone (*Aa–c*), WT subunits and GFP (*Ba–c*) or R424H mutant subunits and GFP (*Ca–c*; see Methods). Green fluorescent protein fluorescence was enhanced by immunostaining with guinea-pig anti-GFP antibody and AlexaFluor (AF) 488-conjugated goat anti-guinea-pig antibody. Purkinje cells were visualized by immunolabelling with rabbit anti-calbindin antibody (red signals in *A–C*). *Ac′*, *Bc′* and *Cc′*, granule cells were selectively immunolabelled with mouse anti-NeuN mouse antibody (see Supplemental Fig. S3*A* and *B*). *D*, relative cell density of PCs plotted as a function of days *in vitro* (DIV). The density was normalized to the value of PCs expressing GFP alone at DIV 4. *E*, relative cell density of granule cells at DIV 14. The density was normalized to the mean cell density of granule cells in cultures lentivirally expressing GFP alone at DIV 14. *F* and *G*, R424H mutant-expressing PCs exhibiting chromatin condensation. *F*, representative fluorescence images of PCs at DIV 8. For nucleus detection, the PCs were stained with Hoechst 33342. Normal nuclei of PCs are indicated by arrows (GFP and WT), whereas a nucleus exhibiting chromatin condensation is marked with an arrowhead (R424H). *G*, summary of the percentages of PCs with chromatin condensation at DIV 8. The statistical analysis was conducted using Student's unpaired *t* tests. In the following figures and tables, the statistical analysis was conducted between cells expressing the R424H mutant and those expressing GFP or between cells expressing R424H mutant and those expressing WT subunits. $^{**}P < 0.01$ and $^{***}P < 0.001$.

not affect the survival of granule cells. The difference in cell survival between PCs and granule cells may be because cultured granule cells do not express endogenous mKv3.3 protein (Supplemental Fig. S3*C*), and R424H mutant subunits were thus unable to form multimeric channels with the endogenous mKv3.3 subunits in the cells (see Discussion). These results indicate that R424H mutant subunits induced PC death and worsened their survival in a day-dependent manner.

To examine the cell death-induced morphological defects in the nuclei of PCs, cerebellar cultures expressing GFP alone, WT mKv3.3 or the R424H mutant were stained with Hoechst 33342 at DIV 8 (Fig. 2*F*). Chromatin in nuclei of GFP- or WT-expressing PCs was stained moderately, with some small bright granules (Fig. 2*F*, arrows in GFP and WT panels), demonstrating normal nuclear morphology. In contrast, PCs expressing R424H mutant subunits showed clear chromatin condensation (Fig. 2*F*, arrowhead in R424H panel). The percentages of PCs exhibiting this chromatin condensation were significantly different between R424H mutant-expressing PCs and the control group (Fig. 2*G*; $P < 0.001$ by Student's unpaired t test). These results suggest that the expression of R424H mutant subunits might induce apoptotic cell death in PCs.

At DIV 7, several neurites were observed in GFP- and WT-expressing PCs, which had morphologies similar to those of R424H mutant-expressing PCs at this stage (Fig. 3*Aa′*, *Ba′* and *Ca′*). However, at DIV 11, GFP- and WT-expressing PCs had elongated immature dendrites, whereas R424H mutant-expressing PCs did not show dendritic extension (Fig. 3*Ab′*, *Bb′* and *Cb′*). Sholl analyses of the dendritic arbors revealed that the number of dendritic intersections in R424H mutant-expressing PCs was significantly smaller than that in GFP-expressing (Fig. 3*D*, at distances of 10–50 μm from the cell body; $P < 0.01$) or WT-expressing PCs (Fig. 3*D*, at distances of 10–40 μm; $P < 0.01$). These results clearly demonstrate that in addition to the induction of cell death, expression of R424H mutant subunits in PCs decreases the survival rate and impairs dendritic development.

R424H mutant-expressing PCs exhibit lower outward current density

The results using *Xenopus* oocytes showed that expression of R424H mutant subunits significantly modulated WT mKv3.3 channel function (Fig. 1 and Supplemental Fig. S2). Thus, similar effects would be predicted in PCs lentivirally expressing R424H mutant subunits. In order to determine how these electrophysiological properties were affected, whole-cell patch-clamp recordings were performed using cultured PCs expressing GFP only, WT subunits or R424H mutant subunits at DIV 8–10.

Purkinje cells could be identified by their large cell bodies (cell body diameters of PCs at DIV 10, 17.2 ± 2.6 μm, $n = 78$; those of other neurons, 7.26 ± 1.7 μm, $n = 226$), and the recordings were confirmed by a combination of intracellular staining and immunocytochemical staining (Supplemental Fig. S4*A*). The cell capacitance of R424H mutant-expressing PCs was significantly lower than that of GFP- or WT-expressing PCs (Table 1; $P < 0.001$ in R424H *versus* GFP and in R424H *versus* WT), reflecting the impairment of dendritic development (Fig. 3*D*). However, the resting membrane potential and input resistance of R424H mutant-expressing PCs showed no difference when

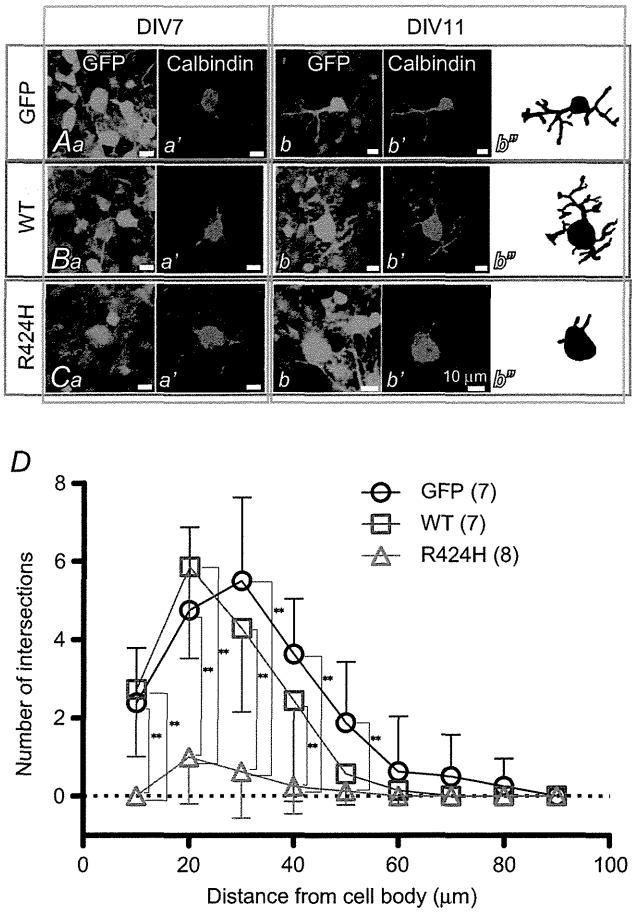

Figure 3. R424H mutant-expressing PCs exhibit impaired dendritic development
A–C, immunofluorescence images of PCs expressing GFP alone (*Aa–b′*), WT subunits and GFP (*Ba–b′*) and R424H mutant subunits and GFP (*Ca–b′*). *Ab″*, *Bb″* and *Cb″*, morphology of PCs expressing GFP (*Ab″*), WT subunits and GFP (*Bb″*) and R424H mutant subunits and GFP (*Cb″*) are depicted for clarity. Each PC was traced using Neurolucida software. *D*, summary of dendrite complexity measured by Sholl analysis. Concentric spheres were centred on the cell body, and the radii were incremented by 10 μm. The number of branching points within each sphere was plotted as dendrite complexity (i.e. the number of intersections). $^{**}P < 0.01$.

Table 1. Basic electrophysiological properties of Purkinje cells

	Membrane capacitance (pF)[a,d]	Resting membrane potential (mV)[a]	Input resistance (MΩ)[a,d]	Percentage of cells showing spontaneous action potentials[b,e]	Frequency of spontaneous action potentials (Hz)[c,e]
GFP alone	39.2 ± 24.3 ($n = 35$)	−58.3 ± 13.6 ($n = 35$)	379 ± 278 ($n = 35$)	80% (12 of 15 cells)	0.43 ± 1.00 ($n = 15$)
WT mKv3.3	40.1 ± 16.1 ($n = 17$)	−59.9 ± 8.24 ($n = 17$)	367 ± 181 ($n = 17$)	75% (6 of 8 cells)	0.25 ± 0.59 ($n = 8$)
R424H mutant	22.3 ± 6.9*† ($n = 28$)	−59.5 ± 7.4 ($n = 28$)	372 ± 169 ($n = 28$)	64% (9 of 14 cells)	0.12 ± 0.75 ($n = 14$)

Here and in Table 2, statistical analysis was conducted between cells expressing the R424H mutant and those expressing green fluorescent protein (GFP) alone or between cells expressing R424H mutant and those expressing wild-type (WT) mKv3.3. Data are given as the means ± SD, and n is the number of experiments. *$P < 0.001$ between GFP alone and R424H mutant. †$P < 0.001$ between WT mKv3.3 and R424H mutant. The statistical analysis indicated by superscript letters a, b and c was conducted using Student's unpaired t test, the χ^2 test and Mann–Whitney U test, respectively. [d]Membrane capacitance and input resistance were measured in voltage-clamp conditions. [e]Spontaneous action potentials were recorded at resting membrane potential for 300 s.

compared with PCs expressing GFP alone or those expressing WT subunits (Table 1; resting membrane potential, R424H *versus* GFP, $P = 0.533$; R424H *versus* WT, $P = 0.874$; and input resistance, R424H *versus* GFP, $P = 0.882$; R424H *versus* WT, $P = 0.913$; analyses by Student's unpaired t test). Spontaneous action potentials were also observed in some PCs in all groups (Table 1 and Supplemental Fig. S4*B* and *C*). The percentages of PCs generating spontaneous firing and the frequency of the firing were comparable among the three groups (Table 1).

Outward currents were recorded in Hepes-buffered ACSF containing TTX, $CdCl_2$, picrotoxin and DNQX (see Methods). Representative current traces recorded from GFP-, WT- and R424H mutant-expressing PCs are illustrated in Fig. 4*A*. Depolarizing voltage pulses (more positive than −10 mV) evoked outward currents with a transient peak in GFP-, WT- and R424H mutant-expressing PCs (Fig. 4*A*). In WT-expressing PCs, peak amplitudes of the transient currents were larger than those in GFP-expressing PCs, indicating that lentivirally expressed mKv3.3 formed functional channels (Fig. 4*Ab*). In contrast, the peak amplitudes in R424H mutant-expressing PCs were smaller than those in GFP-expressing PCs (Fig. 4*Aa* and *Ac*). As the membrane capacitance of R424H mutant-expressing PCs was significantly smaller than that of GFP- and WT-expressing PCs (Table 1), the peak current amplitudes at voltages between +10 and +40 mV were normalized to membrane capacitances (current densities, in pico-amperes per picofarad; Fig. 4*B*). The current densities in R424H mutant-expressing PCs were ∼2-fold smaller than those in GFP-expressing PCs at voltages between +10 and +40 mV (Fig. 4*B*), confirming that the expression of the R424H mutant subunits in cultured PCs suppressed outward currents in a dominant-negative manner.

Expression of R424H mutant subunits reduces sEPSCs in PCs

In standard culture conditions, PCs receive excitatory synaptic inputs from granule cells via the dendrites (Hirano *et al.* 1986; Hirano & Kasono, 1993). In order to examine how R424H mutant-induced impairment of dendritic development affects the synaptic inputs to PCs, sEPSCs were recorded from PCs in the presence of picrotoxin at a holding potential of −80 mV (Fig. 5). Examples of sEPSCs in GFP- or WT-expressing PCs appear as downward deflections in the current traces (Fig. 5*Aa* and *Ba*). These currents were abolished by application of 20 μM DNQX (traces not shown) and were thus identified as being mediated by AMPA/kainate receptors. Ensemble averages of the events in individual cells are also shown in Fig. 5*Ab* and *Bb*. Although sEPSCs in both groups were observed in all cells tested (Table 2), most R424H mutant-expressing PCs (10 of 13 cells) did not show sEPSCs during the 250 s recording period (Fig. 5*C* and Table 2; R424H and GFP, $P < 0.001$; R424H and WT, $P < 0.001$ by Fisher's exact probability test). Even in PCs showing sEPSCs, the frequency was significantly lower than in GFP- or WT-expressing PCs (Table 2). The R424H mutant-expressing PCs might receive few, if any, excitatory synaptic contacts onto their somata and dendrites.

R424H mutant-expressing PCs exhibit broadened action potentials and altered firing patterns

Expression of R424H mutant subunits in PCs suppressed outward current density, suggesting the alteration of the action potential waveform and firing properties in R424H mutant-expressing PCs. To examine these possibilities,

single action potentials (Fig. 6) and repetitive firings (Fig. 7) were evoked in current-clamp conditions. When a single action potential was evoked by short current injection (10 ms duration), R424H mutant-expressing PCs showed a broadened action potential waveform (Fig. 6*A*). The half-amplitude widths of R424H mutant-expressing PCs were 1.7-fold larger than those of GFP-expressing PCs (Fig. 6*B*; $P < 0.001$). The maximal rate of rise and maximal rate of fall in R424H mutant-expressing PCs were 0.75- and 0.65-fold of those in GFP-expressing PCs, respectively (Fig. 6*C* and *D*; maximal rate of rise, $P < 0.001$; maximal rate of fall, $P < 0.001$). These changes suggest that not only outward K^+ current but also voltage-dependent Na^+ current (I_{Na}) was affected by the expression of R424H mutant, because the maximal rate of rise of the action potential has been used as an index of the inward I_{Na} (Hodgkin & Katz, 1949).

To clarify the reduction of the maximal rate of rise by R424H mutant expression, I_{Na} was recorded from PCs in voltage-clamp conditions (Supplemental Fig. S5). Expression of R424H mutant subunits significantly reduced I_{Na} compared with the control group, without any changes in the voltage dependence of activation and inactivation. As the I_{Na} of cultured PCs is distributed through the cell body and axons (Fry *et al.* 2007), the reduction in I_{Na} would be due to the smaller cell body (Table 1, 'Membrane capacitance') and impaired neurite extension of R424H-expressing PCs. The expression of R424H mutant subunits did not affect the threshold current, threshold potential or action potential amplitude of PCs compared with expression of GFP (Fig. 6*E–G*). These results strongly suggest that expression of R424H mutant subunits inhibited the activation of the endogenous mKv3.3 channels, resulting in a reduction of the maximal rate of fall and then in the broadening of action potential duration in PCs.

We next examined the firing properties evoked by long current injection (200 ms duration). Most GFP-expressing PCs (82.9%) showed tonic firing of action potentials (tonic type) in response to depolarizing current injection (Fig. 7*A* and filled column of GFP in Fig. 7*E*), which is consistent with previous reports on the firing pattern of cultured PCs (Tabata *et al.* 2000; Harada *et al.* 2006). The other PCs (17.1%) showed a few spikes (up to three spikes) in response to current injection ranging from 0 to 200 pA

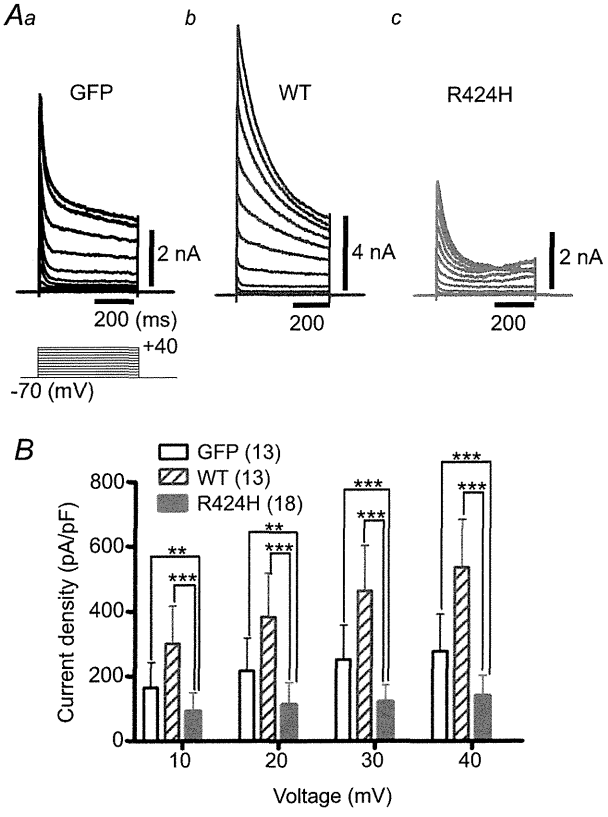

Figure 4. R424H mutant-expressing PCs exhibit suppressed peak outward current density
A, representative outward current traces recorded from PCs expressing GFP alone (*Aa*), WT subunits (*Ab*; note the vertical scale bar) and R424H mutant subunits (*Ac*). The currents were evoked by voltage steps from the −70 mV holding potential to voltages ranging from −60 to +40 mV in 10 mV increments. Leak currents were subtracted online by the *P*/4 protocol. The currents were recorded at DIV 8–10 in Hepes-buffered srtificial cerebrospinal fluid (ACSF) containing TTX, $CdCl_2$, picrotoxin and 6,7-dinitroquinoxaline-2,3-dione (DNQX). *B*, summary of the peak outward current density, which was calculated by dividing the peak outward current by membrane capacitance. $^{**}P < 0.01$ and $^{***}P < 0.001$.

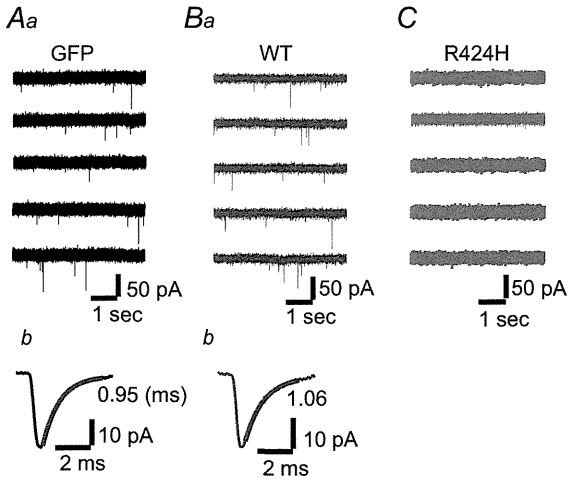

Figure 5. Absence of spontaneous excitatory postsynaptic currents (sEPSCs) in R424H mutant-expressing PCs
Aa, *Ba* and *C*, representative current traces recorded from PCs expressing GFP alone (*Aa*), WT subunits (*Ba*) or R424H mutant subunits (*C*). The sEPSCs appear as downward deflections in *Aa* and *Ba*. The PCs were held at −80 mV in the presence of picrotoxin. *Ab* and *Bb*, averaged sEPSCs from the same cell as in *Aa* and *Ba*, with superimposed single exponential fit. The decay time constant is indicated beside each trace.

Table 2. Summary of spontaneous excitatory postsynaptic current (sEPSC) properties in Purkinje cells

	Percentage of cells showing sEPSCs[a]	Amplitude (pA)[b]	Frequency (Hz)[b]	10–90% Rise time (ms)[b]	Decay time constant (ms)[c]
GFP alone	100%	33.7 ± 9.3	0.62 ± 0.35	0.18 ± 0.04	0.84 ± 0.27
($n = 15$; 1502 events)	(15 of 15 cells)	($n = 15$)	($n = 15$)	($n = 15$)	($n = 15$)
WT mKv3.3	100%	34.0 ± 12.0	0.73 ± 0.35	0.19 ± 0.03	0.87 ± 0.19
($n = 10$; 1041 events)	(10 of 10 cells)	($n = 10$)	($n = 10$)	($n = 10$)	($n = 10$)
R424H mutant	23%	23.1 ± 4.2	0.15 ± 0.10	0.20 ± 0.02	1.14 ± 0.21
($n = 3$; 103 events)	(3 of 13 cells)**††	($n = 3$)	($n = 3$)*†	($n = 3$)	($n = 3$)

All measurements were performed at a holding potential of −80 mV. The statistical analyses indicated by superscript letters a and b were conducted using Student's unpaired *t* test and Fisher's exact probability test, respectively. [c]The sEPSC decay phases were fitted with a single exponential function. *$P < 0.05$, **$P < 0.001$ between GFP alone and R424H mutant. †$P < 0.05$, ††$P < 0.001$ between WT mKv3.3 and R424H mutant.

in 20 pA increments and did not fire tonically during the 200 ms depolarizing pulses (onset type; open column of GFP in Fig. 7*E*). However, approximately half of the R424H mutant-expressing PCs exhibited onset-type firing (53.6%; Fig. 7*C* and *E*), and the remaining PCs exhibited tonic-type firing (46.4%; Fig. 7*D* and *E*). The percentages of firing types in R424H mutant-expressing PCs differed significantly from those in GFP- and WT-expressing PCs (Fig. 7*E*; $P < 0.001$ in both pairs by the χ^2 test). The firing frequencies of tonic-type neurons in the three groups were plotted against the injected current (Fig. 7*F*). Wild-type-expressing PCs showed the highest frequencies, in the range of 40–200 pA (Fig. 7*B* and *F*), demonstrating that lentivirally expressed WT subunits contributed to the generation of narrow action potentials by accelerating the falling phase (Fig. 7*A* and *D* and Supplemental Fig. S3*E*). In tonic-type neurons, firing frequencies in R424H mutant-expressing PCs were significantly lower than those in GFP-expressing PCs, in the range of 180–200 pA (Fig. 7*F*; $P < 0.05$ at 180 and 200 pA depolarization). These results demonstrate that expression of R424H mutant subunits changed the ratio of tonic-firing PCs and reduced PC excitability in response to depolarization.

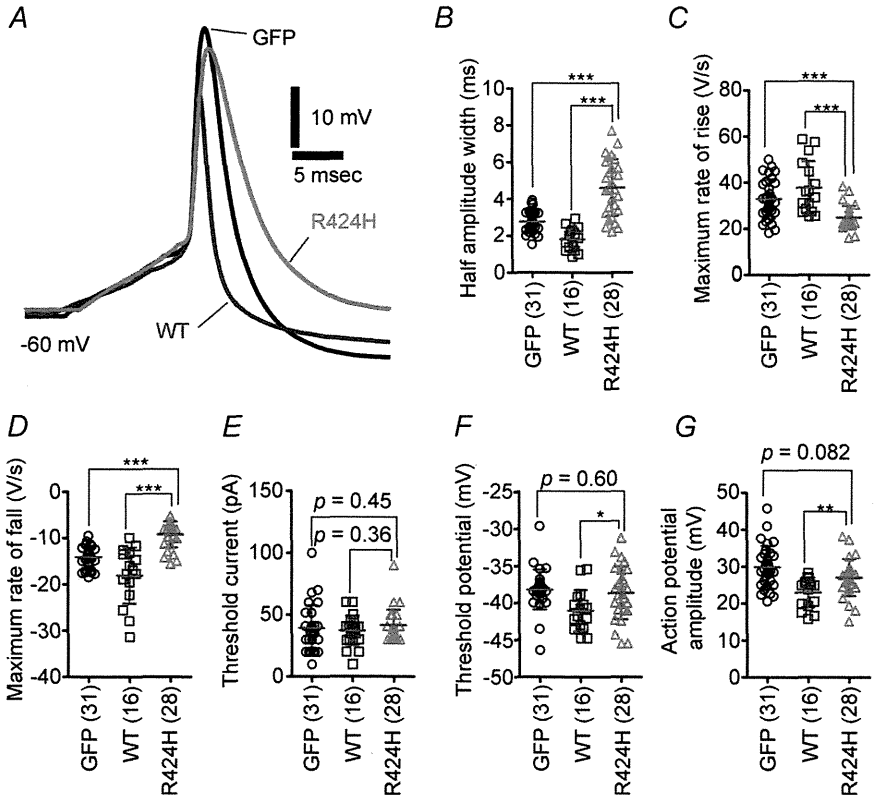

Figure 6. R424H mutant-expressing PCs exhibit broadened action potential waveforms
A, representative single action potential waveforms of PCs. The action potentials were evoked by short depolarizing current injection (10 ms duration). Action potentials were aligned by superimposing the rising phase of each trace. The resting membrane potentials were adjusted to −60 mV by current injection.
B–*G*, comparison of action potential properties. *B*, half-amplitude width measured at the mid-point between the threshold and peak of the action potential. *C* and *D*, maximal rate of rise (*C*) and of fall (*D*) of action potentials. *E*, threshold current amplitude. *F*, threshold potential. *G*, action potential amplitude, as measured between the threshold and peak. *$P < 0.05$, **$P < 0.01$ and ***$P < 0.001$.

R424H mutant-expressing PCs show higher $[Ca^{2+}]_i$, and blockade of P/Q-type Ca^{2+} channels rescues the PC death and dendritic maldevelopment caused by the mutant subunits

The expression of R424H mutant subunits in cerebellar cultures caused PC death. We hypothesized that the cell death was caused by excessive Ca^{2+} influx through the following steps. As cultured PCs spontaneously generate action potentials, which increase basal $[Ca^{2+}]_i$ (Schilling *et al.* 1991; Supplemental Fig. S4*B* and *C* and Table 1), the broadening of action potentials by R424H mutant expression would cause increased Ca^{2+} influx via excessive activation of voltage-gated Ca^{2+} channels. This influx would lead to a defect of Ca^{2+} homeostasis in PCs, resulting in the cell death as a part of a stress response (Orrenius *et al.* 2003). Indeed, excessive Ca^{2+} influx triggered by the blockade of K^+ channels has been shown to induce cell death in several types of cells (Kim *et al.* 2000; Lajdova *et al.* 2004; Wang *et al.* 2011). To test this hypothesis, we performed calcium imaging (Fig. 8) and then rescue experiments of PC death using ω-agatoxin IVA, a specific blocker for the P/Q-type voltage-gated Ca^{2+} channels that mediate predominant Ca^{2+} currents in PCs (Mintz & Bean, 1993; Gillard *et al.* 1997; Fig. 9).

Calcium imaging was performed using cerebellar cultures loaded with fura-2 AM (see Methods). After a baseline recording (measurement of basal $[Ca^{2+}]_i$) for 8 min, cerebellar cultures were depolarized for 5 min by perfusion of high-K^+ ACSF (Fig. 8*B*). In basal conditions, $[Ca^{2+}]_i$ in R424H mutant-expressing PCs was approximately four times higher than in the control group (Fig. 8*Ca*; $P < 0.001$ in R424H *versus* GFP and in R424H *versus* WT). There were no significant differences in high-K^+-induced $[Ca^{2+}]_i$ elevation (~200 nM) between PCs expressing the R424H mutant and those expressing GFP alone or expressing WT subunits (Fig. 8*Cb*). The basal $[Ca^{2+}]_i$ of granule cells infected with the

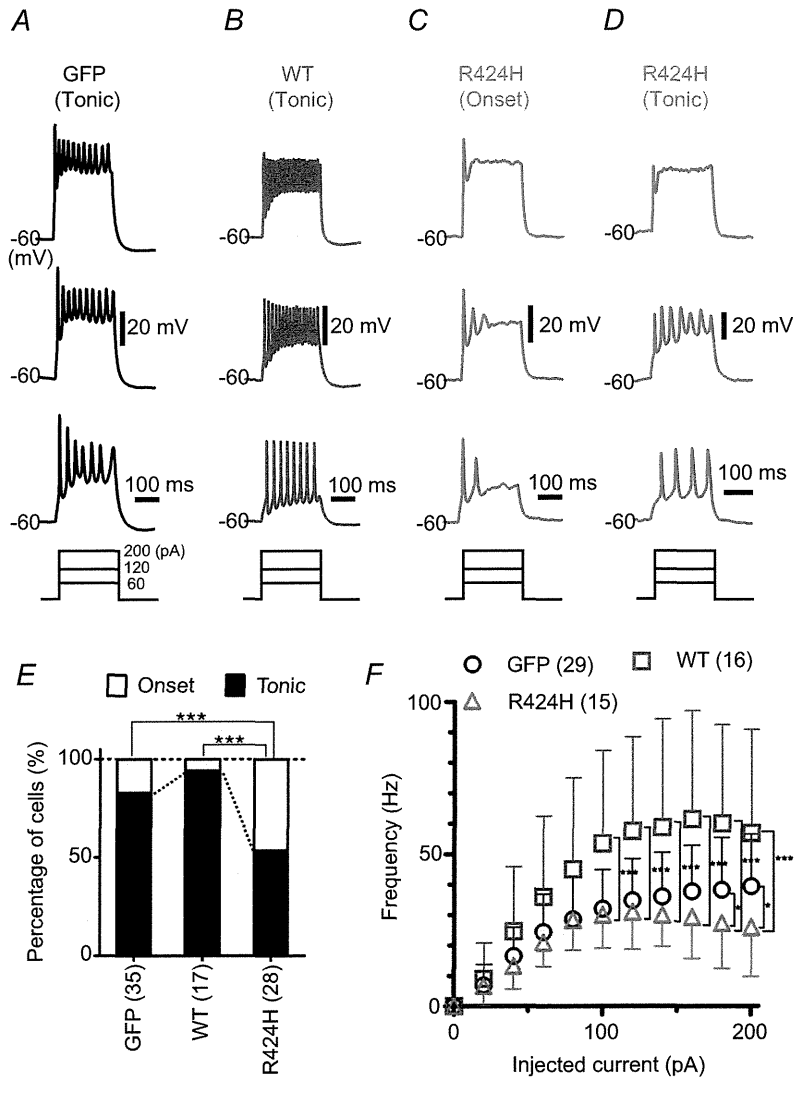

Figure 7. R424H mutant-expressing PCs exhibit altered firing patterns
A–D, representative firing patterns of PCs expressing GFP alone (*A*), WT subunits (*B*) or R424H mutant subunits (*C* and *D*). Approximately half of the R424H mutant-expressing PCs fired at the onset of current injection (onset-type; *C*). The action potentials were evoked by long depolarizing current injection (200 ms duration). The resting membrane potentials were adjusted to −60 mV. *E*, comparison of firing patterns. The χ^2 test was used for the statistical analyses. *F*, the firing frequency of the tonic-type cells is plotted as a function of injected current. $^*P < 0.05$ and $^{***}P < 0.001$.

lentiviruses was also measured, and there were no significant differences between R424H mutant-expressing and control cultures (GFP, 71.2 ± 41.2 nM, $n = 86$; WT, 69.7 ± 38.0 nM, $n = 118$; R424H, 63.6 ± 32.9 nM, $n = 72$; $P = 0.365$ between GFP and R424H; $P = 0.423$ between WT and R424H).

To examine whether the elevated basal $[Ca^{2+}]_i$ induced PC death in R424H mutant-expressing cultures, we performed a similar experiment to that in Fig. 2. In this experiment, ω-agatoxin IVA (0.2 μM) was added to the culture medium at DIV 2 (see Methods), and WT-expressing cultures were omitted to simplify the experimental design. Treatment of GFP-expressing cultures with ω-agatoxin IVA did not affect relative PC density (Fig. 9*D*, filled circles) but increased the branch number and the total length of dendrites at DIV 14 (Fig. 9*E* and *F*; filled circles in Fig. 9*I* and *J*), in good agreement with a previous report (Schilling *et al.* 1991; see Discussion). Treatment of R424H mutant-expressing cultures with ω-agatoxin IVA significantly increased relative PC density at DIV 11 and 14 (Fig. 9*D*, red triangles) and significantly rescued dendritic development in PCs (Fig. 9*G* and *H*; red triangles in Fig. 9*I* and *J*). These results clearly indicate that P/Q-type Ca^{2+} channels play a critical role in the PC death and impairment of dendrite development caused by R424H mutant expression, and support our hypothesis.

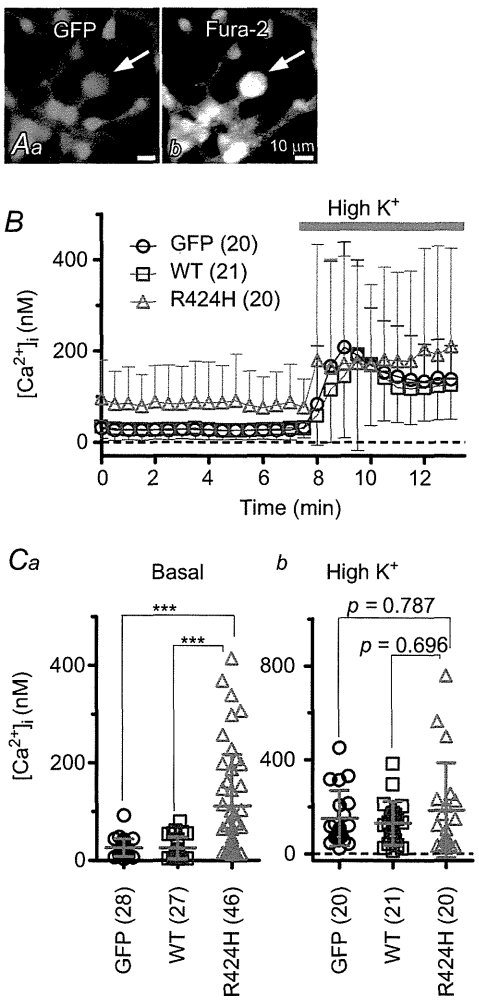

Figure 8. Significantly higher basal $[Ca^{2+}]_i$ in PCs expressing R424H mutant
A, representative fluorescence images of a fura-2 AM-loaded cerebellar culture expressing GFP alone. Arrows indicate PCs. *Aa*, GFP fluorescence (excitation, 470–495 nm; emission, 510–550 nm). *Ab*, fura-2 fluorescence (excitation, 375–385 nm; emission, 470–550 nm). *B*, the time course of free $[Ca^{2+}]_i$ in PCs. To depolarize PCs, high-K^+ ACSF (High K^+) was bath applied during the time indicated by the grey bar. *C*, summary of averaged $[Ca^{2+}]_i$ in PCs. Basal $[Ca^{2+}]_i$ was obtained as the average of a 7 min period from the beginning of the recordings (*Ca*), and elevated $[Ca^{2+}]_i$ from a 5 min period during high-K^+ ACSF perfusion (*Cb*). ***$P < 0.001$.

Discussion

In this study, we found that the expression of R424H mutant subunits in cerebellar cultures significantly impaired dendritic development and survival in PCs (Figs 2 and 3). Prior to cell death, R424H mutant-expressing PCs showed broadened action potential waveforms, altered firing properties and elevated basal $[Ca^{2+}]_i$ (Figs 6–8). Moreover, chronic inhibition of P/Q-type Ca^{2+} channels by ω-agatoxin IVA rescued the PC death and dendritic maldevelopment caused by expression of R424H mutant subunits (Fig. 9). This is the first report to show that a missense mutation found in SCA13 patients induces maldevelopment of PC dendrites and eventually PC death, most probably due to elevated basal $[Ca^{2+}]_i$ in PCs.

Biophysical properties of R424H mutant channels

The biophysical properties of hKv3.3 channels with the R423H mutation, which corresponds to the R424H mutation in mKv3.3 channels, have been previously reported (Figueroa *et al.* 2010; Minassian *et al.* 2012). Our results in Supplemental Fig. S2 agreed well with the previous reports and suggest that the properties of R424H mutant mKv3.3 were essentially identical to those of R423H-mutant hKv3.3. Moreover, we found that coexpression of R424H mutant and WT subunits accelerated the inactivation kinetics and slowed recovery from inactivation compared with expression of WT subunits alone (Fig. 1). Therefore, we predict that the properties we found in R424H mutant mKv3.3 are shared with R423H mutant hKv3.3.

We confirmed that homomeric R424H mutant channels showed negligible currents and that R424H mutant subunits exerted a dominant-negative influence on WT mKv3.3 channels in *Xenopus* oocytes (Supplemental Fig. S2*A* and *B*; Figueroa *et al.* 2010, 2011). Very recently,

Zhao *et al.* (2013) reported that in heterologous expression systems using Chinese hamster ovary cells, the surface protein level of R423H mutant hKv3.3 channels is 30% of that of WT hKv3.3 and that the conductance density of the mutant is 16% of that of the WT. Therefore, we cannot exclude the possibility that the reduced surface expression of mKv3.3 channels by the mutation would also contribute to the broadening of action potentials (Fig. 6) and lower firing frequency (Fig. 7) in transduced PCs. However, the reduction of the conductance density cannot be explained fully by the reduced surface protein expression.

To explain the negligible activity and dominant-negative property of R424H mutant channels, we propose two hypothetical mechanisms. First, the positively charged arginine at position 424 in mKv3.3 may be a critical residue in the S4 segment, serving as a part of the voltage sensor domain (Seoh *et al.* 1996). The partial disruption of the sensor domain by R424H mutation would make the subunits less sensitive to membrane voltage changes, resulting in the loss of channel function. Second, an arginine residue at position 174 in the S4 segment of KAT1, which is a voltage-gated K^+ channel in *Arabidopsis*, plays an essential role in the appropriate integration of the S3 and S4 segment into the endoplasmic reticulum membrane (Sato *et al.* 2003). Given that the R174 is homologous to R424 in mKv3.3, defective membrane insertion of R424H mutant subunits could occur in *Xenopus* oocytes, leading to a defect in channel activity.

Purkinje cell death by R424H mutant expression and the inhibition by blockade of P/Q-type voltage-gated Ca^{2+} channels

In this study, we revealed that expression of R424H mutant subunits caused cell death and impaired dendritic growth in PCs (Figs 2 and 3) and that these effects were reversed by the blockade of P/Q-type Ca^{2+} channels (Fig. 9). Addition of ω-agatoxin IVA also enhanced dendritic elongation in PCs expressing GFP alone (Fig. 9*E* and *F*; filled circles in Fig. 9*I* and *J*). Together with a previous report showing that chronic application of TTX in cerebellar cultures caused dendritic elongation in PCs (Schilling *et al.* 1991), activation of P/Q-type Ca^{2+} channels by neuronal activity may adversely influence dendritic elongation in PCs. Addition of ω-agatoxin IVA in R424H mutant-expressing cultures did not completely restore PC survival rates

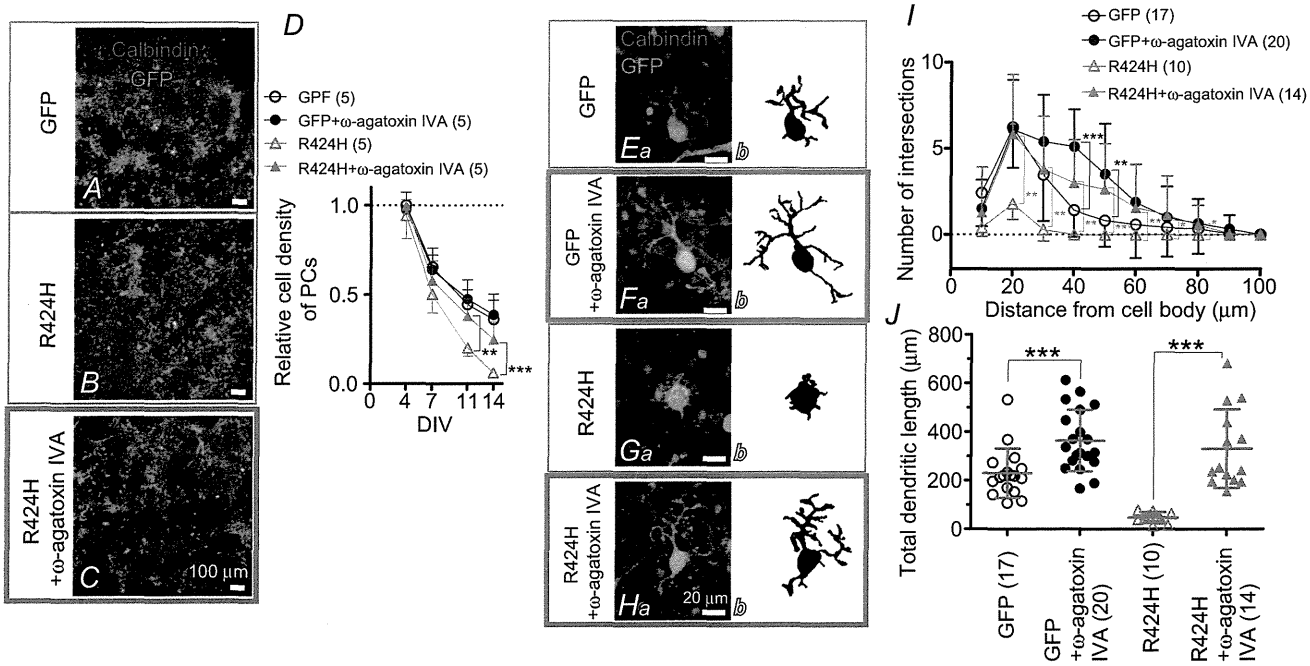

Figure 9. Pharmacological blockade of P/Q-type Ca^{2+} channels rescues the PC death and dendritic maldevelopment caused by expression of R424H mutant
A–C, cerebellar cultures expressing GFP alone (*A*) or R424H mutant with GFP (*B* and *C*). The cultures were immunostained for calbindin at DIV 14. In *C*, ω-agatoxin IVA was added to the culture medium every other day from DIV 2. *D*, relative cell density of PCs plotted as a function of DIV. The density was normalized to the value of PCs expressing GFP alone at DIV 4. *E–H*, calbindin-immunolabelled PCs expressing GFP alone (*Ea* and *Fa*) or R424H mutant subunits with GFP (*Ga* and *Ha*) at DIV 14. Morphologies of PCs are depicted in the right-hand panels for clarity. In *F* and *H*, ω-agatoxin IVA was added. *I*, and *J*, summary of dendrite complexity measured by Sholl analysis (*I*) and of total dendritic length (*J*). $^*P < 0.05$, $^{**}P < 0.01$, and $^{***}P < 0.001$.

(Fig. 9*D*). This may be because some Ca^{2+} currents in cultured PCs are mediated by Ca^{2+} channels other than the P/Q-type (Gillard *et al.* 1997), and activation of these channels may contribute to PC death. We therefore performed the same rescue experiments using $CdCl_2$ (0.2 mM; a non-selective Ca^{2+} channel blocker) or a combination of ω-agatoxin IVA and verapamil hydrochloride (0.02 mM; an L-type Ca^{2+} channel blocker), but these chemicals markedly deteriorated the viability and development of cerebellar cultures within 3 DIV (data not shown).

In contrast to PCs, there were no significant decreases in the numbers of granule cells upon R424H mutant expression (Fig. 2*E*). This may be because granule cells do not express endogenous mKv3.3 channels with which R424H mutant subunits form oligomeric channels (Supplemental Fig. S3*C*), resulting in the absence of the dominant-negative influence on the endogenous channels by the expression of mutant channel subunits.

Comparison with preceding papers on Kv3.3 knockout mice and zebrafish expressing mutant Kv3.3

In contrast to the impaired dendritic development in R424H mutant-expressing PCs (Fig. 3*Cb′* and *D*), the cerebellum of Kv3.3 knockout mice shows neither dendritic shrinkage of PCs nor cerebellar atrophy (Zagha *et al.* 2010). Furthermore, the knockout mice display only moderate motor dysfunction and no ataxic phenotype, although SCA13 patients show severe ataxia (Joho *et al.* 2006; Hurlock *et al.* 2008; Waters & Pulst, 2008; Figueroa *et al.* 2010). This difference may be attributable to the following factors. In PCs, mKv3.3 is thought to form heteromultimeric channels by assembling with Kv3.1 and/or Kv3.4 (Goldman-Wohl *et al.* 1994; Weiser *et al.* 1994), and Kv3 channels contribute to repolarization of both somatic Na^+ spikes and dendritic Ca^{2+} spikes (McKay & Turner, 2004). Genetic elimination of Kv3.3 subunits may be insufficient to exhibit the dendritic shrinkage and severe ataxia phenotypes because of functional compensation by Kv3.1 and Kv3.4 in PCs (Goldman-Wohl *et al.* 1994; Weiser *et al.* 1994; Martina *et al.* 2003). We detected the expression of Kv3.4 subunits in cultured PCs (Supplemental Fig. S3*D*). It is therefore reasonable to hypothesize that R424H mutant subunits form heteromultimeric channels not only with endogenous mKv3.3 but also with other members of Kv3.3, including Kv3.4, resulting in total inhibition of the K^+ channel activity in PCs. This may account for the differences in the morphological phenotypes of PCs in our results *versus* the knockout mice.

Zebrafish expressing infant-onset mutant zebrafish Kv3.3 (homologous to the F448L mutant in SCA13 patients) in spinal motoneurons show defective axonal pathfinding (Issa *et al.*, 2012). Indeed, the zebrafish is an interesting model for understanding the effects of mutant Kv3.3 expression in spinal motoneurons. However, as they used a motoneuron-specific enhancer of *Mnx1* (*Hb9*) gene, the exogenous proteins were not expressed in the cerebellar neurons. To examine the effects of mutant Kv3.3 in the cerebellum, it would be necessary to express the mutant protein directly in the cerebellar neurons using a different method.

Comparison of our culture results with SCA13 patients harbouring the R423H mutation

Spinocerebellar ataxia type 13 patients harbouring the R423H mutation generally show early-onset, slow-progressive ataxia and cerebellar atrophy (Figueroa *et al.* 2010, 2011). Our immunohistochemical analyses demonstrated that expression of R424H mutant subunits impaired dendritic development and induced cell death in cultured PCs (Figs 2 and 3). Those defects may be responsible for the cerebellar atrophy and ataxia observed in SCA13 patients, although it is necessary to verify that similar impairments are also observed in post-mortem cerebellum of the patients.

In functional aspects, we found that expression of R424H mutant subunits significantly decreased outward current mediated by voltage-gated K^+ channels, reduced sEPSCs, broadened action potentials and altered firing properties (Figs 4–7 and Table 2), suggesting the existence of similar functional changes in SCA13 patients. As PCs are the sole output neurons from the cerebellar cortex and make inhibitory synaptic contacts directly onto neurons in the deep cerebellar nuclei and the vestibular nuclei in the brainstem, PCs play crucial roles in motor co-ordination (Zheng & Raman, 2010). Accordingly, it is easily assumed that the reduction of spontaneous excitatory inputs and the changed firing properties in PCs disrupt synaptic transmission to neurons in the deep cerebellar nuclei and vestibular nuclei, resulting in impaired motor co-ordination. To examine the effects of the R424H mutation on electrophysiological properties of PCs and animal behaviour, we tried expressing R424H mutant subunits in PCs *in vivo* by directly injecting the virus solution into mouse cerebellar cortex as described in our previous papers (Torashima *et al.* 2006, 2008; Shuvaev *et al.* 2011). However, despite the presence of the infection, sufficient overexpression of mKv3.3 channels and apparent ataxia were not observed (data not shown). This may be because endogenous mKv3.3 proteins are abundantly expressed in PCs and the overexpression failed to reach the endogenous protein level. Efficient reduction of K^+ currents in PCs *in vivo* as observed in cultured PCs may be attained by using a different type of viral vector, such as adeno-associated virus vectors (Nathanson *et al.* 2009). Alternatively, K^+ currents in PCs *in vivo* may be effectively decreased using viral vector-mediated

expressions of R424H mutant subunits in *Kv3.3*$^{-/-}$ or *Kv3.3*$^{+/-}$ mice, which express no mKv3.3 proteins or only half the normal amount.

Currently, three different missense mutations in hKv3.3 channels have been reported from distinct pedigrees, and the disease onset and clinical phenotypes also differ among them (Waters *et al.* 2006; Figueroa *et al.* 2010, 2011). In the present study, we focused on only one mutation (R423H in hKv3.3) because of the drastic changes it induced in channel properties in the *Xenopus* oocyte expression system and its early-onset phenotype in SCA13 patients. Further studies of the effects of other mutants (R420H and F448L in hKv3.3) on cultured PCs may provide explanations for the differences in the disease phenotypes.

Possible significance of this study

We developed an *in vitro* SCA13 model using mouse cerebellar cultures and lentivirus vector-mediated gene expression. This model has advantages over *in vivo* models, such as transgenic mice, in the ease of controlling culture conditions by applying chemical compounds. Therefore, this model would be useful in screening drugs for SCA13 and in detailed investigations of the signalling cascades that promote the observed cell death. Given that blockade of P/Q-type Ca^{2+} channels rescued the phenotypes found in this research, the channel blockers may be potential therapeutic drugs for SCA13. Furthermore, this culture method, in combination with virus-mediated gene expression, may be applicable to the study of other types of hereditary spinocerebellar ataxia.

References

Armstrong CM & Bezanilla F (1974). Charge movement associated with the opening and closing of the activation gates of the Na channels. *J Gen Physiol* **63**, 533–552.

Ashcroft FM (2006). From molecule to malady. *Nature* **440**, 440–447.

Chang SY, Zagha E, Kwon ES, Ozaita A, Bobik M, Martone ME, Ellisman MH, Heintz N & Rudy B (2007). Distribution of Kv3.3 potassium channel subunits in distinct neuronal populations of mouse brain. *J Comp Neurol* **502**, 953–972.

Costa PF, Emilio MG, Fernandes PL, Ferreira HG & Ferreira KG (1989). Determination of ionic permeability coefficients of the plasma membrane of *Xenopus laevis* oocytes under voltage clamp. *J Physiol* **413**, 199–211.

Desai R, Kronengold J, Mei J, Forman SA & Kaczmarek LK (2008). Protein kinase C modulates inactivation of Kv3.3 channels. *J Biol Chem* **283**, 22283–22294.

Drummond GB (2009). Reporting ethical matters in *The Journal of Physiology*: standards and advice. *J Physiol* **587**, 713–719.

Erisir A, Lau D, Rudy B & Leonard CS (1999). Function of specific K^+ channels in sustained high-frequency firing of fast-spiking neocortical interneurons. *J Neurophysiol* **82**, 2476–2489.

Figueroa KP, Minassian NA, Stevanin G, Waters M, Garibyan V, Forlani S, Strzelczyk A, Bürk K, Brice A, Dürr A, Papazian DM & Pulst SM (2010). KCNC3: phenotype, mutations, channel biophysics—a study of 260 familial ataxia patients. *Hum Mutat* **31**, 191–196.

Figueroa KP, Waters MF, Garibyan V, Bird TD, Gomez CM, Ranum LP, Minassian NA, Papazian DM & Pulst SM (2011). Frequency of KCNC3 DNA variants as causes of spinocerebellar ataxia 13 (SCA13). *PLoS One* **6**, e17811.

Fry M, Boegle AK & Maue RA (2007). Differentiated pattern of sodium channel expression in dissociated Purkinje neurons maintained in long-term culture. *J Neurochem* **101**, 737–748.

Gillard SE, Volsen SG, Smith W, Beattie RE, Bleakman D & Lodge D (1997). Identification of pore-forming subunit of P-type calcium channels: an antisense study on rat cerebellar Purkinje cells in culture. *Neuropharmacology* **36**, 405–409.

Gimenez-Cassina A, Lim F & Diaz-Nido J (2007). Gene transfer into Purkinje cells using herpesviral amplicon vectors in cerebellar cultures. *Neurochem Int* **50**, 181–188.

Goldman-Wohl DS, Chan E, Baird D & Heintz N (1994). Kv3.3b: a novel Shaw type potassium channel expressed in terminally differentiated cerebellar Purkinje cells and deep cerebellar nuclei. *J Neurosci* **14**, 511–522.

Grynkiewicz G, Poenie M & Tsien RY (1985). A new generation of Ca^{2+} indicators with greatly improved fluorescence properties. *J Biol Chem* **260**, 3440–3450.

Hanawa H, Hematti P, Keyvanfar K, Metzger ME, Krouse A, Donahue RE, Kepes S, Gray J, Dunbar CE, Persons DA & Nienhuis AW (2004). Efficient gene transfer into rhesus repopulating hematopoietic stem cells using a simian immunodeficiency virus-based lentiviral vector system. *Blood* **103**, 4062–4069.

Harada KH, Ishii TM, Takatsuka K, Koizumi A & Ohmori H (2006). Effects of perfluorooctane sulfonate on action potentials and currents in cultured rat cerebellar Purkinje cells. *Biochem Biophys Res Commun* **351**, 240–245.

Hawley RG, Lieu FH, Fong AZ & Hawley TS (1994). Versatile retroviral vectors for potential use in gene therapy. *Gene Ther* **1**, 136–138.

Hille B (2001). *Ion Channels of Excitable Membranes*. Sinauer, Sunderland, MA.

Hirai H & Launey T (2000). The regulatory connection between the activity of granule cell NMDA receptors and dendritic differentiation of cerebellar Purkinje cells. *J Neurosci* **20**, 5217–5224.

Hirano T & Kasono K (1993). Spatial distribution of excitatory and inhibitory synapses on a Purkinje cell in a rat cerebellar culture. *J Neurophysiol* **70**, 1316–1325.

Hirano T, Kubo Y & Wu MM (1986). Cerebellar granule cells in culture: monosynaptic connections with Purkinje cells and ionic currents. *Proc Natl Acad Sci U S A* **83**, 4957–4961.

Hodgkin AL & Katz B (1949). The effect of sodium ions on the electrical activity of giant axon of the squid. *J Physiol* **108**, 37–77.

Hurlock EC, McMahon A & Joho RH (2008). Purkinje-cell-restricted restoration of Kv3.3 function restores complex spikes and rescues motor coordination in *Kcnc3* mutants. *J Neurosci* **28**, 4640–4648.

Issa FA, Mock AF, Sagasti A & Papazian DM (2012). Spinocerebellar ataxia type 13 mutation that is associated with disease onset in infancy disrupts axonal pathfinding during neuronal development. *Dis Model Mech* **5**, 921–929.

Joho RH, Street C, Matsushita S & Knöpfel T (2006). Behavioral motor dysfunction in Kv3-type potassium channel-deficient mice. *Genes Brain Behav* **5**, 472–482.

Kim JA, Kang YS, Jung MW, Kang GH, Lee SH & Lee YS (2000). Ca^{2+} influx mediates apoptosis induced by 4-aminopyridine, a K^+ channel blocker, in HepG2 human hepatoblastoma cells. *Pharmacology* **60**, 74–81.

Kubo Y & Murata Y (2001). Control of rectification and permeation by two distinct sites after the second transmembrane region in Kir2.1 K^+ channel. *J Physiol* **531**, 645–660.

Lajdova I, Chorvat D Jr, Spustova V & Chorvatova A (2004). 4-Aminopyridine activates calcium influx through modulation of the pore-forming purinergic receptor in human peripheral blood mononuclear cells. *Can J Physiol Pharmacol* **82**, 50–56.

McKay BE & Turner RW (2004). Kv3 K^+ channels enable burst output in rat cerebellar Purkinje cells. *Eur J Neurosci* **20**, 729–739.

MacKinnon R (1991). Determination of the subunit stoichiometry of a voltage-activated potassium channel. *Nature* **350**, 232–235.

Martina M, Yao GL & Bean BP (2003). Properties and functional role of voltage-dependent potassium channels in dendrites of rat cerebellar Purkinje neurons. *J Neurosci* **23**, 5698–5707.

Mellor JR, Merlo D, Jones A, Wisden W & Randall AD (1998). Mouse cerebellar granule cell differentiation: electrical activity regulates the $GABA_A$ receptor $\alpha 6$ subunit gene. *J Neurosci* **18**, 2822–2833.

Mikuni T, Uesaka N, Okuno H, Hirai H, Deisseroth K, Bito H & Kano M (2013). Arc/Arg3.1 is a postsynaptic mediator of activity-dependent synapse elimination in the developing cerebellum. *Neuron* **78**, 1024–1035.

Minassian NA, Lin MC & Papazian DM (2012). Altered Kv3.3 channel gating in early-onset spinocerebellar ataxia type 13. *J Physiol* **590**, 1599–1614.

Mintz IM & Bean BP (1993). Block of calcium channels in rat neurons by synthetic omega-Aga-IVA. *Neuropharmacology* **32**, 1161–1169.

Mullen RJ, Buck CR & Smith AM (1992). NeuN, a neuronal specific nuclear protein in vertebrates. *Development* **116**, 201–211.

Nathanson JL, Yanagawa Y, Obata K & Callaway EM (2009). Preferential labelling of inhibitory and excitatory cortical neurons by endogenous tropism of adeno-associated virus and lentivirus vectors. *Neuroscience* **161**, 441–450.

Orrenius S, Zhivotovsky B & Nicotera P (2003). Regulation of cell death: the calcium–apoptosis link. *Nat Rev Mol Cell Biol* **4**, 552–565.

Rae JL & Shepard AR (2000). Kv3.3 potassium channels in lens epithelium and corneal endothelium. *Exp Eye Res* **70**, 339–348.

Rudy B & McBain CJ (2001). Kv3 channels: voltage-gated K^+ channels designed for high-frequency repetitive firing. *Trends Neurosci* **24**, 517–526.

Sato M, Suzuki K, Yamazaki H & Nakanishi S (2005). A pivotal role of calcineurin signalling in development and maturation of postnatal cerebellar granule cells. *Proc Natl Acad Sci U S A* **102**, 5874–5879.

Sato Y, Sakaguchi M, Goshima S, Nakamura T & Uozumi N (2003). Molecular dissection of the contribution of negatively and positively charged residues in S2, S3, and S4 to the final membrane topology of the voltage sensor in the K^+ channel, KAT1. *J Biol Chem* **278**, 13227–13234.

Sawada Y, Kajiwara G, Iizuka A, Takayama K, Shuvaev AN, Koyama C & Hirai H (2010). High transgene expression by lentiviral vectors causes maldevelopment of Purkinje cells in vivo. *Cerebellum* **9**, 291–302.

Schilling K, Dickinson MH, Connor JA & Morgan JI (1991). Electrical activity in cerebellar cultures determines Purkinje cell dendritic growth patterns. *Neuron* **7**, 891–902.

Seoh SA, Sigg D, Papazian DM & Bezanilla F (1996). Voltage-sensing residues in the S2 and S4 segments of the *Shaker* K^+ channel. *Neuron* **16**, 1159–1167.

Sholl DA (1953). Dendritic organization in the neurons of the visual and motor cortices of the cat. *J Anat* **87**, 387–406.

Shuvaev AN, Horiuchi H, Seki T, Goenawan H, Irie T, Iizuka A, Sakai N & Hirai H (2011). Mutant PKCγ in spinocerebellar ataxia type 14 disrupts synapse elimination and long-term depression in Purkinje cells *in vivo*. *J Neurosci* **31**, 14324–14334.

Szymczak AL, Workman CJ, Wang Y, Vignali KM, Dilioglou S, Vanin EF & Vignali DA (2004). Correction of multi-gene deficiency in vivo using a single 'self-cleaving' 2A peptide-based retroviral vector. *Nat Biotechnol* **22**, 589–594.

Tabata T, Sawada S, Araki K, Bono Y, Furuya S & Kano M (2000). A reliable method for culture of dissociated mouse cerebellar cells enriched for Purkinje neurons. *J Neurosci Methods* **104**, 45–53.

Takayama K, Torashima T, Horiuchi H & Hirai H (2008). Purkinje-cell-preferential transduction by lentiviral vectors with the murine stem cell virus promoter. *Neurosci Lett* **443**, 7–11.

Torashima T, Iizuka A, Horiuchi H, Mitsumura K, Yamasaki M, Koyama C, Takayama K, Iino M, Watanabe M & Hirai H (2009). Rescue of abnormal phenotypes in $\delta 2$ glutamate receptor-deficient mice by the extracellular N-terminal and intracellular C-terminal domains of the $\delta 2$ glutamate receptor. *Eur J Neurosci* **30**, 355–365.

Torashima T, Koyama C, Iizuka A, Mitsumura K, Takayama K, Yanagi S, Oue M, Yamaguchi H & Hirai H (2008). Lentivector-mediated rescue from cerebellar ataxia in a mouse model of spinocerebellar ataxia. *EMBO Rep* **9**, 393–399.

Torashima T, Okoyama S, Nishizaki T & Hirai H (2006). In vivo transduction of murine cerebellar Purkinje cells by HIV-derived lentiviral vectors. *Brain Res* **1082**, 11–22.

Wang W, Xiao J, Adachi M, Liu Z & Zhou J (2011). 4-Aminopyridine induces apoptosis of human acute myeloid leukemia cells via increasing $[Ca^{2+}]_i$ through P_2X_7 receptor pathway. *Cell Physiol Biochem* **28**, 199–208.

Waters MF, Minassian NA, Stevanin G, Figueroa KP, Bannister JP, Nolte D, Mock AF, Evidente VG, Fee DB, Müller U, Dürr A, Brice A, Papazian DM & Pulst SM (2006). Mutations in voltage-gated potassium channel KCNC3 cause degenerative and developmental central nervous system phenotypes. *Nat Genet* **38**, 447–451.

Waters MF & Pulst SM (2008). SCA13. *Cerebellum* **7**, 165–169.

Weiser M, Vega-Saenz de Miera E, Kentros C, Moreno H, Franzen L, Hillman D, Baker H & Rudy B (1994). Differential expression of Shaw-related K^+ channels in the rat central nervous system. *J Neurosci* **14**, 949–972.

Zagha E, Manita S, Ross WN & Rudy B (2010). Dendritic Kv3.3 potassium channels in cerebellar Purkinje cells regulate generation and spatial dynamics of dendritic Ca^{2+} spikes. *J Neurophysiol* **103**, 3516–3525.

Zhao J, Zhu J & Thornhill WB (2013). Spinocerebellar ataxia-13 Kv3.3 potassium channels: arginine-to-histidine mutations affect both functional and protein expression on the cell surface. *Biochem J* **454**, 259–265.

Zheng N & Raman IM (2010). Synaptic inhibition, excitation, and plasticity in neurons of the cerebellar nuclei. *Cerebellum* **9**, 56–66.

Additional Information

Competing interests

None declared.

Author contributions

T.I. and H.H. conceived and designed experiments. T.I. and Y.M. performed experiments. T.I. collected and analysed data. T.I., Y.S. and H.H. wrote the paper.

Funding

This work was supported by Health Labour Sciences Research Grant (T.I.), JSPS KAKENHI grant numbers 24790230 (T.I.) and 19670003 (H.H.), and JSPS Funding Program for Next Generation World-Leading Researchers (LS021 to H.H.).

Acknowledgements

The lentiviral vector and MSCV promoter were provided by St Jude Children's Research Hospital and the American National Red Cross, respectively. We thank Dr L. K. Kaczmarek for mouse Kv3.3 cDNA and Dr K. Nakajo for technical advice and valuable comments on electrophysiological recording from *Xenopus* oocytes.

The Journal of Toxicological Sciences (J. Toxicol. Sci.)
Vol.38, No.3, ***-***, 2013

Toxicomics Report

Comparative gene expression analysis of the amygdala in autistic rat models produced by pre- and post-natal exposures to valproic acid

Atsuko Oguchi-Katayama[1], Akihiko Monma[2], Yuko Sekino[1], Toru Moriguchi[2] and Kaoru Sato[1]

[1]Laboratory of Neuropharmacology, Division of Pharmacology, National Institute of Health Sciences, 1-18-1 Kamiyoga, Setagaya-ku, Tokyo 158-8501, Japan
[2]Department of Food and Life Sciences, Azabu University, 1-17-71 Fuchinobe, Tyuoku, Sagamihara-shi, Kanagawa 252-5201, Japan

(Received October 24, 2012; Accepted March 14, 2013)

ABSTRACT — Gene expression profiles in the amygdala of juvenile rats were compared between the two autistic rat models for mechanistic insights into impaired social behavior and enhanced anxiety in autism. The rats exposed to VPA by intraperitoneal administration to their dams at embryonic day (E) 12 were used as a model for autism (E2IP), and those by subcutaneous administration at postnatal day (P) 14 (P14SC) were used as a model for regressive autism; both of the models show impaired social behavior and enhanced anxiety as symptoms. Gene expression profiles in the amygdala of the rats (E12IP and P14SC) were analyzed by microarray and compared to each other. Only two genes, Neu2 and Mt2a, showed significant changes in the same direction in both of the rat models, and there were little similarities in the overall gene expression profiles between them. It was considered that gene expression changes per se in the amygdala might be an important cause for impaired social behavior and enhanced anxiety, rather than expression changes of particular genes.

Key words: Valproic acid, Amygdala, Microarray, Prenatal, Postnatal

INTRODUCTION

There are two similar but different kinds of autistic animal models produced by perinatal exposure of rodents to valproic acid (VPA). Rodents exposed to VPA on embryonic day (E) 12 have been used as an animal model for autism characterized by impaired social behavior, enhanced anxiety, and decreased sensitivity to pain after maturation (Markram *et al.*, 2008; Schneider and Przewtocki, 2005; Schneider *et al.*, 2007, 2008). On the other hand, rodents exposed to VPA on postnatal day (P) 14 have been used as an animal model for regressive autism that shows impaired social behavior like animal models for autism but accompanied by loss of some acquired skills (Yochum *et al.*, 2008, 2010; Wagner *et al.*, 2006). The regressive autism model also showed enhanced anxiety in our preliminary study.

The amygdala has been considered critical for behaviors associated with emotional disorders. Possible mechanisms of impaired social behavior in autism involve neural networks including the amygdala (Neuhaus *et al.*, 2010). The amygdala has also been identified to be involved in anxiety behaviors (Blackford and Pine, 2012). In humans, the amygdala and prefrontal cortex is the responsible for anxiety disorders (Etkin and Wager, 2007). It is therefore expected that comparative analysis of the amygdala in the two animal models for autism provide some mechanistic insights into impaired social behavior and enhanced anxiety in autism from similarities between them.

In the present study, we performed comparative gene expression analysis of the amygdala and characterize the similarities between the animal models for autism and for regressive autism. We first confirmed the effect of postnatal exposure to VPA on anxiety-related behavior in rats. We then compared gene expression profiles in the amygdala of juvenile rats between prenatal and postnatal exposures to VPA.

Correspondence: Kaoru Sato (E-mail: kasato@nihs.go.jp)

MATERIALS AND METHODS

Animals and VPA treatment

Pregnant Wistar Hannover/Rcc rats were obtained from Japan SLC, Inc. (Shizuoka, Japan) and maintained individually under conventional conditions with controlled temperature (23 ± 3°C) and illumination (12 hr; 7:00-19:00). Each of five litters was culled to 10 pups/litter on day 2 after birth for matched nursing conditions. For postnatal exposure, saline or 400 mg/kg of VPA (Sigma, St. Louis, MO, USA) was administered subcutaneously (s.c.) to half of the pups in each litter on postnatal day 14 (P14SC). For prenatal exposure, saline or 600 mg/kg of VPA was administered intraperitoneally (i.p.) to five pregnant rats on E12 (E12IP). Microarray analysis was performed at 5 (E12IP and P14SC) or 7 (P14SC7w) wks after the VPA administrations (Fig. 1). All animal treatments and experimental protocols were approved by the Animal Care and Use Committee of the Azabu University and the National Institute of Health Science (NIHS), and followed the Guide for the Care and Use of Laboratory Animals.

Behavioral test for anxiety

As a behavioral test, elevated plus maze (EPM) was performed in P14SC at 5 wks old with a maze consists of two opposite open arms (50 × 10 cm) and two opposite enclosed arms. The arms are connected by a central 10-cm square, forming a plus shape. The maze was elevated 50 cm above the floor. The animal's path was observed for 5 min after a resting period of 2 min in the central square of the maze. The number of entries into the open arms and the time spent in the open arms were measured.

Microarray analysis

Microarray analysis was performed using animals different from those used for behavioral test. The amygdalae were removed from the juvenile rats, and incubated in a RNA stabilization solution (RNAlater, Ambion, Austin, TX, USA) (1 ml for 5 x 5 x 5 (mm) block) overnight. Total RNA samples from the amygdalae were isolated with TRIzol (Invitrogen, Carlsbad, CA, USA) and the RNeasy Mini Kit (Qiagen, Hilden, Germany), with slight modifications to the manufacturer's protocol. The

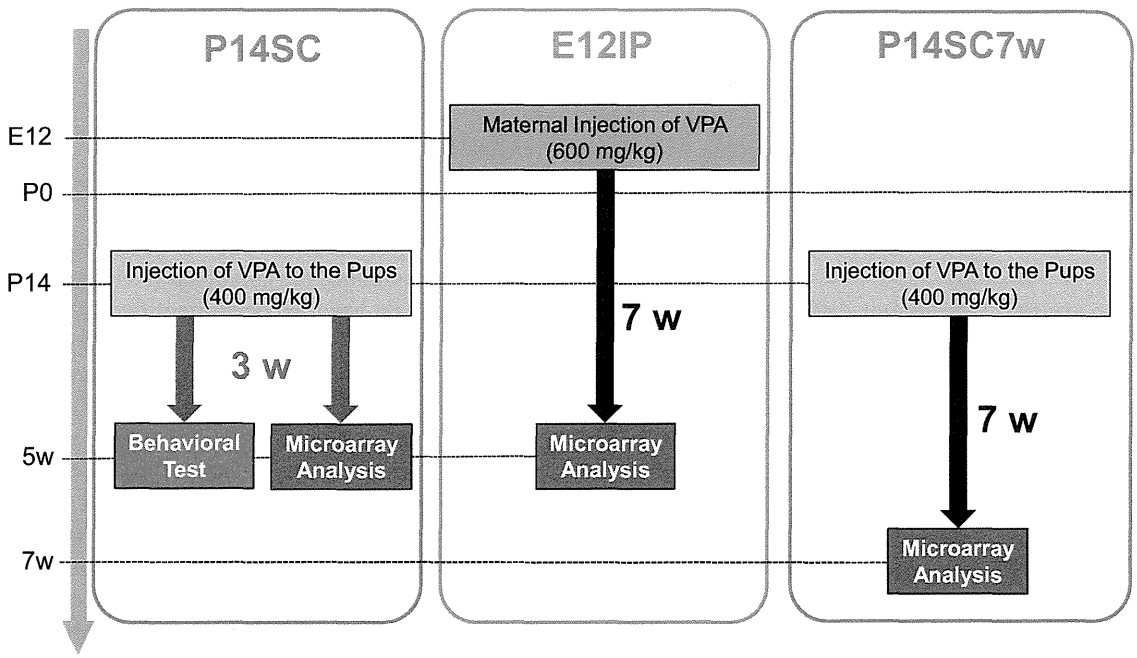

Fig. 1. The experimental design. To investigate the effect of postnatal VPA exposure on behavior and gene expression profiles, saline or 400 mg/kg VPA was administered to half of the pups per one litter subcutaneously on postnatal day 14 (P14SC). Behavior test and microarray analysis were performed using individual animals. To avoid influence of the dams, 5w juvenile rats (P35-37) were obtained evenly from 5 litters for control group and VPA- treated group, respectively. To investigate the effect of prenatal exposure, five pregnant rats were treated intraperitoneally (i.p.) with saline or 600 mg/kg VPA on E12.5 (E12IP), respectively, and microarray analysis was performed at 5w (P35-37). To analyze the contribution of the length of time from VPA exposure to cRNA isolation to the change in gene expression profile, microarray analysis was also performed at 7w (P49-56) (5 w after VPA exposure at P14) (P14SC7w).

isolated RNA sample (100 μg) were used for the microarray analysis (Affymetrix GeneChip Rat Genome 230 2.0 array (Santa Clara, CA, USA)) according to the Affymetrix protocol (http://www.affymetrix.com/support/technical/manuals.affx). Data were collected using Affymetrix GeneChip® Operating Software (GCOS) (http://media.affymetrix.com/support/technical/whitepapers/sadd_whitepaper.pdf).

Data analysis

Data analyses were carried out with GeneSpring (Agilent Technologies, Santa Clara, CA, USA). All of the data from the VPA-treated groups were normalized to the median of the control groups, and the expression of each selected gene was calculated as a log ratio of the signal to the control value. To assess the differences between the control and VPA-treated groups, the Benjamini and Hochberg false-discovery rate (FDR) method was employed, and those with a p-value less than 0.05 were considered as significant. Network, function, and pathway analyses were performed using Ingenuity Pathway Analysis software (IPA; Ingenuity Systems, Redwood City, CA, USA).

RESULTS AND DISCUSSION

Behavioral tests for anxiety

The time spent in the open arms was significantly shorter in the males of P14SC than in those of the corresponding control, indicating enhanced anxiety by postnatal exposure to VPA (Fig. 2, left). There were, however, no significant changes in the behavior test of the females (Fig. 2, right). There were no effects of the VPA exposure on the number of entries into the open arms in both genders (data not shown). These results indicate that postnatal exposure to VPA caused enhanced anxiety specifically in males. This sexual dimorphism is a typical feature of autism and has been observed in the animal model for autism produced by prenatal exposure to VPA (Schneider *et al.*, 2008). We therefore analyzed the gene expression profile of the amygdala exposed to VPA only in males in the following experiments.

Gene expression microarray analysis

In the controls, gene expression profiles were almost identical among the varied VPA exposure conditions. The number of genes with expression levels different from those in the corresponding controls was larger in P14SC (53 probe sets for 49 genes) than in E12IP (32 probe sets for 30 genes), excluding expressed sequence tags (Fig. 3A). Functional classification of the genes also indicated the differences of gene expression between P12IP and P14SC (Fig. 3B). P14SC contained a wider variety of categories than E12IP; 'phosphatase' appeared only in E12IP, while 'cytokine', 'growth factor', 'lig-

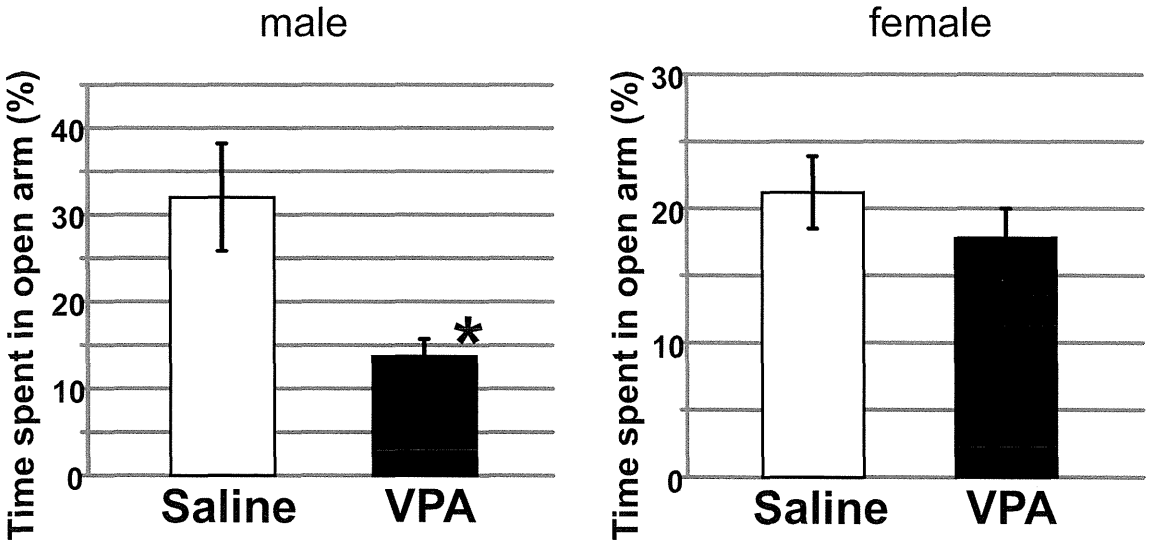

Fig. 2. The effects of postnatal exposure to VPA on anxiety-related behavior. 400 mg/kg VPA was administered to animals subcutaneously at P14. Anxiety-related behaviors were analyzed at 5w by EPM. Total open arm entries and time spent in open arm are quantified. The data of time spent in open arm were shown. An asterisk indicates a statistically significant difference from the control ($P < 0.05$, $N = 13$-15, Student's t test).

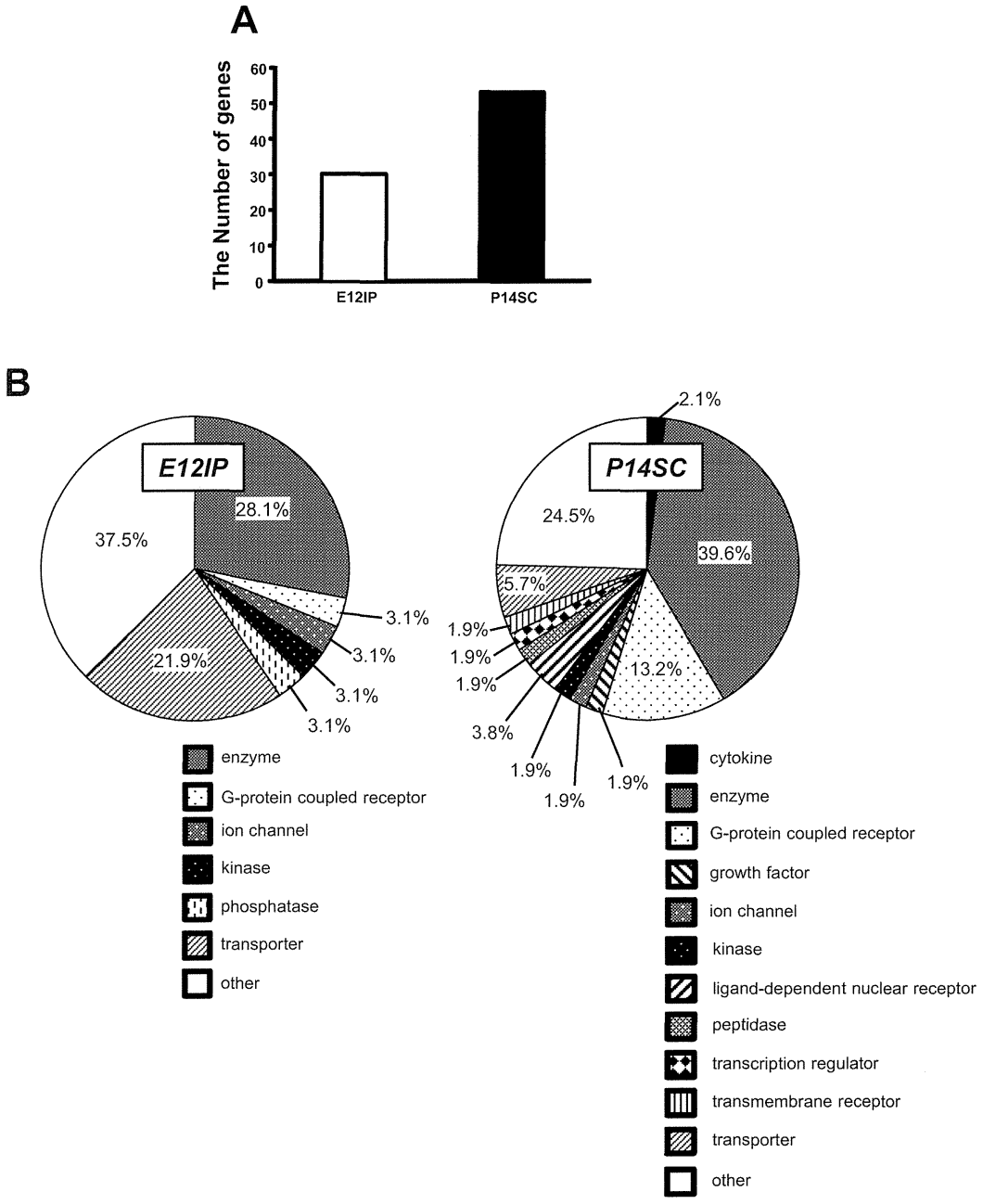

Fig. 3. Summary of the gene expression profiles of E12IP and P14SC rats (male). For both of E12IP and P14SC, total RNA of the amygdalae of 5w male rats (P33-37, N = 4) were analyzed with the microarray chip. Data were collected using Affymetrix GeneChip® Operating Software (GCOS) and analyzed using GeneSpring software. A. The numbers of significantly changed genes in E12IP and P14SC ($p < 0.05$, N = 4). B. Functional classification of the significantly changed genes by GeneSpring.

and-dependent nuclear receptor', 'peptidase', 'transcription regulator', and 'transmembrane receptor' appeared only in P14SC. As for categories common to E12IP and P14SC, their proportions were different from each other; e.g., 'transporters' accounted for 21.9% in E12IP but only 5.7% in P14SC.

Only two genes, Neu2 and Mt2a, exhibited the significant changes in the same direction in E12IP and P14SC

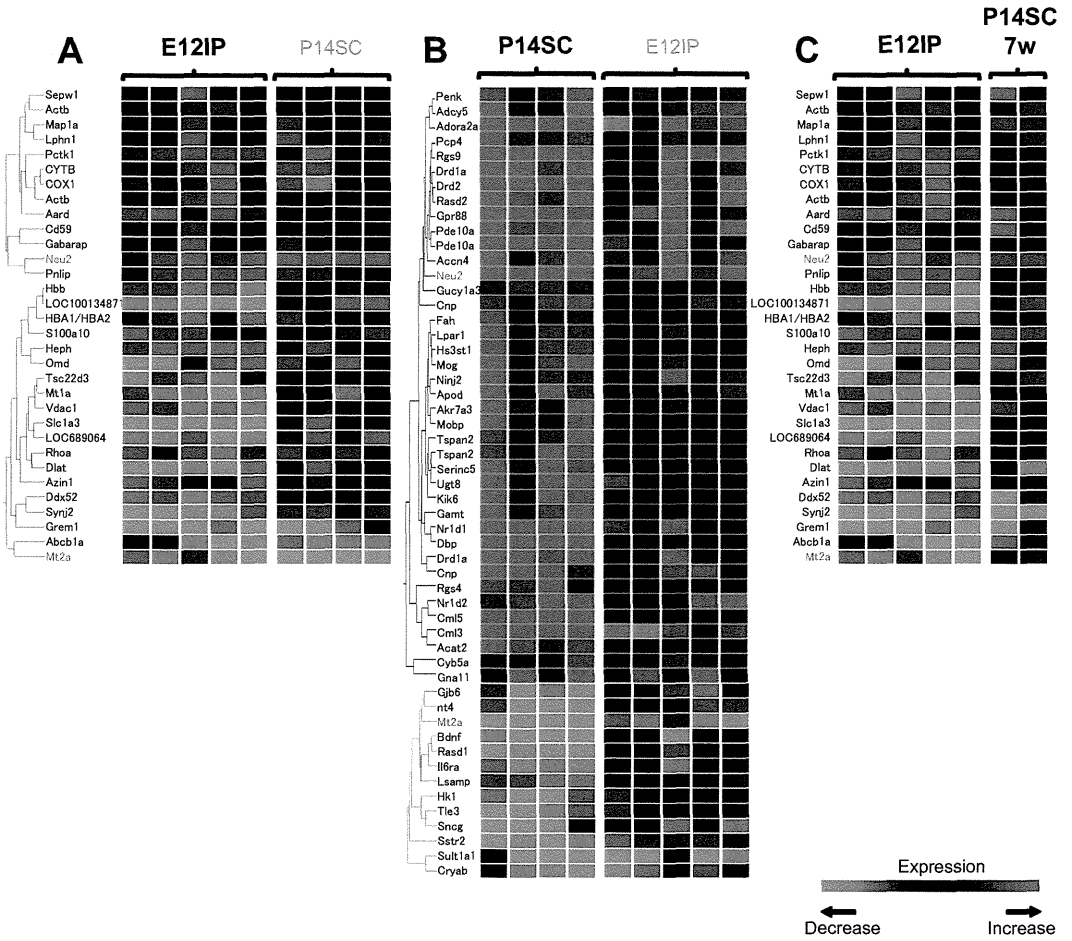

Fig. 4. Heat maps representing hierarchical clustering of the significantly changed genes of E12IP and P14SC. Each vertical column represents an individual sample, and each horizontal row represents a single gene. (N = 4 for P14SC and E12IP, N = 2 for P14SC7w) A. A heat map/hierarchical clustering of the significantly changed genes of E12IP with a heat map of the same genes of P14SC. Clustering was performed using the Benjamini and Hochberg FDR method. B. A heat map/hierarchical clustering of the significantly changed genes of P14SC with a heat map of the same genes of E12IP. C. A heat map of E12IP was compared with that of P14SC7w in which cRNA was extracted 7 w after VPA exposure at P14.

(red letters in Figs. 4A and B). The expression profile in E12IP was also different from that in P14SC7w (Fig. 4C), suggesting that the differences between E12IP and P14SC were not due to the varied length of time between the VPA exposure and the gene expression analysis. Precise gene lists for the heat maps of E12IP (Fig. 4A) and P14SC (Fig. 4B) are shown in Table 1 and Table 2, respectively. 'Behavior'-related genes were identified only in P14SC (Table 3). A larger number of genes were categorized as 'nervous system development and function', 'neurological disease' and 'psychological disorders' in P14SC than in E12IP.

Pathway analysis

The most significantly changed network (Fig. 5A [i]) was that linking 'cell death', 'cellular compromise', and 'neurological disease'. The hubs of this network were MYC, HTT, and CASP3, although the expression levels of these three genes remained unchanged. The second most significantly changed network was that linking 'cell death', 'neurological disease', and 'carbohydrate metabolism' (Fig. 5A [ii]). TNF, which plays an especially important role in cell death, was a highly interconnected node. In P14SC, three significant networks were identified (Fig. 5B [i]-[iii]). These networks are related to 'nucleic acid metabolism' (Fig. 5B [i]), 'cell signaling' (Fig. 5B